Contributions of gravity waves in the ocean to *T*-phase excitation by earthquakes[a)]

Oleg A. Godin[b)]

Department of Physics, Naval Postgraduate School, 833 Dyer Road, Monterey, California 93943-5216, USA

Running title: Abyssal *T*-waves

Keywords: range-dependent waveguides; wave propagation theory; sound scattering; wind waves; sea swell; internal gravity waves

Submitted to the *Journal of the Acoustical Society of America* on July 8, 2021

[a)] Parts of this work have been previously reported at the 178th Meeting of the Acoustical Society of America (San Diego, December 2019).

[b)] Electronic mail: oagodin@nps.edu

Abstract

Generation of *T*-waves in a deep ocean by an earthquake in its epicentral region is often observed but the mechanism of the excitation of the acoustic waves travelling horizontally with the speed of sound remains controversial. Here, the hypothesis is investigated that the abyssal *T*-waves are generated by scattering of ballistic sound waves by surface and internal gravity waves in the ocean. Volume and surface scattering are studied theoretically in the small perturbation approximation. In the 3–50 Hz typical frequency range of the observed *T*-waves, linear internal waves are found to lack the necessary horizontal spatial scales to meet the Bragg scattering condition and contribute appreciably to *T*-wave excitation. In contrast, the ocean surface roughness has the necessary spatial scales at typical sea states and wind speeds. Efficiency of the acoustic normal modes' excitation at surface scattering of the ballistic body waves by wind seas and sea swell is quantified and found to be comparable to that of the established mechanism of *T*-wave generation at downslope conversion at seamounts. The surface scattering mechanism is consistent with key observational features of abyssal *T*-waves, including their ubiquity, low-frequency cutoff, presence on seafloor sensors, and weak dependence on the earthquake focus depth.

PACS numbers: 43.30.Ma, 43.30.Dr, 43.30.Hw, 43.30.Ft, 43.30.Nb

I. INTRODUCTION

The *T*-, or tertiary, phase of an underwater earthquake is composed of low-frequency acoustics waves, which propagate to long ranges in underwater waveguide at speeds close to the sound speed in water and arrive later than *P*-, or primary, and *S*-, or secondary phases, which are due to compressional (*P*) and shear (*S*) body waves in the seabed, and later than seismo-acoustic interface waves.[1–4] *T* waves weakly attenuate with range, travel over very large distances, and are observed throughout the world ocean. They are the most common earthquake sounds in the ocean and make strong but transient contributions to the ambient sound field.[5, 6] A comprehensive review of *T*-wave research up to mid-2000s can be found in Refs. 2, 3, 7, and 8.

In addition to hydrophones at various depths in the water column,[9–13] *T* waves are routinely observed by receivers on the seafloor in deep water,[14–16] which indicates, in agreement with full-wave numerical modeling,[8, 12, 17–19] that *T*-waves are not confined in the SOFAR channel. Because the wave speed and absorption in water are, respectively, smaller and much smaller than in the earth crust, *T* waves prove to be the most sensitive and rather accurate means to detect, characterize, and localize marine teleseismic events, including weak intraplate events.[9, 20–23] In addition, *T* waves carry information about the ocean. It was proposed to use measurements of temporal variability of *T*-wave travel times to characterize internal tides and associated ocean mixing[24] and, more recently, for ocean acoustic thermometry.[25, 26]

Numerous observations show that conversion of seismic energy into guided acoustic waves in oceanic waveguide occurs in the vicinity of the earthquake epicenter and at prominent bathymetric features, which may be located hundreds of kilometers away from the epicenter.[3, 9, 13, 20, 27–31] *T*-wave amplitudes remain significant for intermediate-depth earthquakes[9, 32] and are insensitive to water depth.[2] *T* waves from deep-focus earthquakes, with hypocenter depths of hundreds of km, have been also observed.[3, 14] The conversion mechanism and especially *T*-wave excitation in the immediate vicinity of the epicenter are not well understood.[2, 8, 22] Excitation of acoustic normal modes at large-scale bathymetric features can be explained in terms of the downslope conversion and diffraction of *P* and *S* body waves and/or seismo-acoustic interface waves by horizontally inhomogeneous bathymetry.[8, 19, 33–36] Ubiquitous "abyssal" *T* waves[9, 32, 33, 37] that are generated near the epicenter of earthquakes under flat abyssal planes, cannot be attributed to any of these generation mechanisms. Unlike the trapping of acoustic energy in the SOFAR channel by downslope conversion of steeply propagating sound, generation of abyssal *T* waves does not lend itself to a ray interpretation. It had been realized early on[9, 32, 37] that a wave scattering mechanism was required to explain abyssal *T*-wave observations. Johnson, Norris, and Duennebier discussed scattering at the ocean surface and seafloor and volume scattering of sound in the ocean among the conceivable generation mechanisms and favored scattering by the ocean surface.[9, 32, 37] However, their crude estimates of the generation efficiency were not encouraging. Keenan and Merriam[38] proposed sound scattering from keels on the undersurface of the ice cover as the mechanism of generation of abyssal *T* waves in the Arctic. The idea that sound scattering at the ocean surface could be an important mechanism of *T*-phase generation has been recently re-visited by Bottero[8] using full-wave, two-dimensional (2-D) numerical modeling in a scenario with strong, discrete scatterers located on the ocean surface.

Following Fox et al.[20] and De Groot-Hedlin and Orcutt,[39, 40] it is often implied in the current literature[3, 6, 22] that abyssal *T* waves are generated due to wave scattering by seafloor roughness, specifically due to coupling between the seismo-acoustic normal modes that are directly excited by the seismic source, and the normal modes comprising the *T*-phase.[41, 42] By modeling scattered waves as the field due to uncorrelated virtual sound sources distributed along the seafloor, De Groot-Hedlin and Orcutt[39, 40] and Yang and Forsyth[22] successfully reproduced the shapes of envelopes of observed *T*-phase waveforms. However, detailed information about the seafloor roughness spectra is rarely if ever available around the epicenter of abyssal earthquakes with the granularity and at the spatial scales necessary for *T*-phase modeling. To our knowledge, the amplitude of the resulting *T* waves has never been related to actual seafloor roughness data or models in a quantitative manner and shown to be sufficient to explain the observed abyssal *T* waves.

Here, we examine an alternative hypothesis that sound waves coming at steep angles directly from the earthquake focus (ballistic body waves) are coupled to normal modes of the underwater acoustic waveguide by dynamic processes in the water column and on the ocean surface. Specifically, we investigate the generation of abyssal *T* waves at scattering of ballistic sound waves by the ocean surface roughness, which is due to surface gravity waves, and by volume inhomogeneities of the water column, which are caused by internal gravity waves. We view the ocean surface and volume scattering as either a complementary to the seafloor scattering or possibly an alternative mechanism of generation of abyssal *T* waves. Unlike the seafloor roughness data in the open ocean, extensive information on statistics of wind waves and sea swell[43–45] and internal gravity wave spectra[46, 47] is available, which allows one to reach definitive conclusions regarding significance of these generation mechanisms.

T waves are a seismo-acoustic phenomenon with representative wave frequencies being very high on the seismic scale and low for underwater sound. Typically, *T* waves are observed in the 1–100 Hz band.[2, 3] Lower frequencies dominate the signals from stronger and deeper earthquakes, while the highest frequencies are generated by the weakest detected seismic events. Abyssal *T* waves exhibit higher frequencies than the *T* waves generated at down-slope conversion.[3, 32] Therefore, this paper will focus on the 3–50 Hz frequency band that contains most of the abyssal *T*-wave energy. Observations indicate existence of a low-frequency cutoff in *T*-phase spectra, see, e.g., Refs. 13, 32, 48 and Ref. 8, p. 59. The low-frequency cutoff will be related to the *T*-phase generation process in this paper.

Mathematically, we describe the excitation of abyssal *T*-waves as scattering from the continuous spectrum into the discrete spectrum of the seismo-acoustic field. The continuous spectrum is represented here by the body waves, that are generated by an earthquake and reach the water column with a modest transmission loss at typical *T*-phase frequencies below about 40–50 Hz. This process is reciprocal of scattering of the normal modes propagating in the oceanic waveguide by the rough ocean surface and/or volume inhomogeneities due to internal gravity waves (scattering from the discrete into the continuous spectrum of the acoustic field). In that problem, a part of the scattered energy is radiated into the seabed and carried away from the waveguide, leading to the well-known contribution to attenuation of the normal modes.[49–52]

The remainder of the paper is organized as follows. A theory of excitation of acoustic normal modes at scattering of a low-frequency body wave by rough ocean surface and random volume inhomogeneities is developed in Sec. II for underwater waveguides with either fluid or solid bottom. Efficiency of *T*-phase excitation by ballistic body waves is related to the spectral properties of the roughness and volume inhomogeneities. The theory is applied in Sec. III to surface scattering by wind seas with the Pierson-Moskovitz spectrum and wavetrains of sea swell to characterize the frequency spectra, directionality, and energy of the resulting *T* waves and the dependence of the *T*-phase properties on the earthquake focus depth. Simple, order-of-magnitude estimates of the *T*-phase energy are obtained in Sec. IV A and employed to argue, that surface scattering of ballistic body waves in the vicinity of the earthquake epicenter is a significant *T*-

phase generation mechanism with a strength comparable to that of a seamount at a moderate distance from the epicenter. Section IV B discusses possible extensions of the theory to quantify other plausible mechanisms of generation of *T* waves and related waves in the atmosphere. Section V summarizes our findings.

II. *T*-PHASE GENERATION BY SURFACE AND VOLUME SCATTERING

A. Scattering of low-frequency sound by the rough ocean surface

Consider a horizontally stratified ocean of depth H. Introduce Cartesian coordinates x, y, z with the vertical coordinate z increasing downward. The mean position of the ocean surface is the horizontal plane $z = 0$; the seafloor is located at $z = H$ (Fig. 1). The epicenter of an earthquake, which generates *T* waves, is located in the vicinity of the origin $x = 0$, $y = 0$ of the horizontal coordinates. In addition to the Cartesian coordinates, we will also use a cylindrical coordinate system $\{r, \varphi, z\}$ with the same z axis. When averaged over perturbations due to internal gravity waves, sound speed c in the ocean and water density ρ, as well as the density and compressional and shear wave speeds in the seabed, are functions of z. We disregard the seafloor roughness and the effects of horizontal inhomogeneities of the water column and seabed when considering wave scattering by the ocean surface roughness.

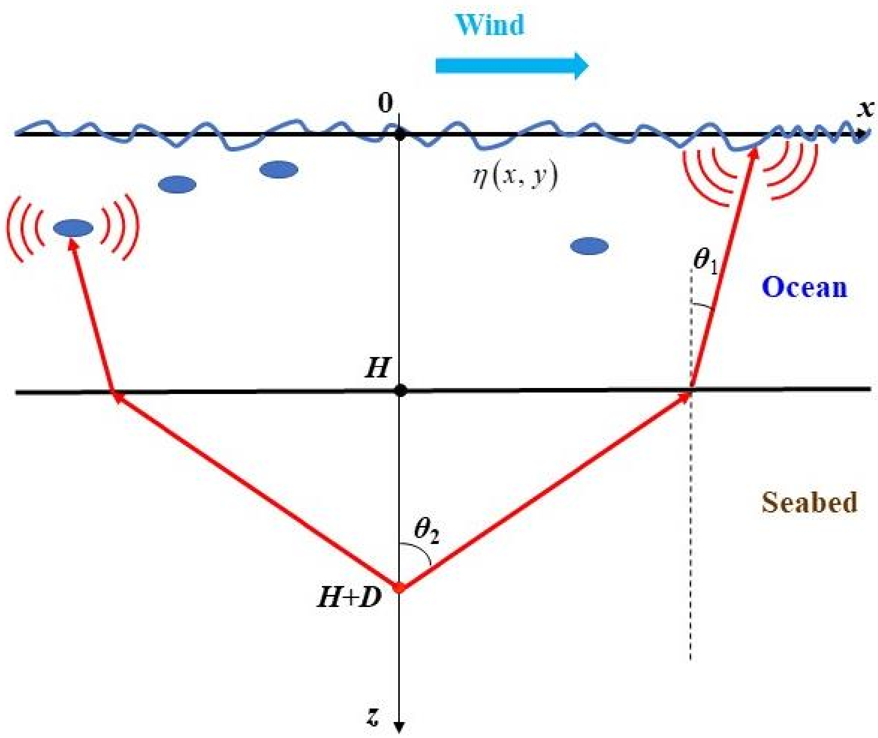

Figure 1. (Color online) Geometry of the problem. Ballistic waves from the earthquake focus scatter at the rough ocean surface and volume inhomogeneities in the water column, which act as secondary sound sources and generate guided waves in the oceanic waveguide. The volume inhomogeneities are symbolically represented by ovals in the figure. The ocean surface roughness is described by the surface elevation η, which varies with the horizontal coordinates x and y. The earthquake focus is located at $x = y = 0$ at the depth $z = H + D$ under the seafloor $z = H$.

Wave heights on the ocean surface are small compared to acoustic wavelengths at *T*-phase frequencies (longer than 30 m for frequencies below 50 Hz). With a possible exception for some breaking waves, slopes of the ocean surface are small compared to unity. Sound scattering by such surfaces can be described by the small perturbation method.[53, 54] Consider scattering of monochromatic acoustic waves of frequency ω by a stationary (frozen) rough surface. We will use complex notation for monochromatic wave fields, where the time dependence $\exp(-i\omega t)$ of the acoustic pressure and other quantities is assumed and suppressed. In the first approximation of the small perturbation method, acoustic pressure p_{sc} in the wave scattered by a rough pressure-release surface is

$$p_{sc}\left(\mathbf{R}\right)=-\int\left[\frac{\partial p_0}{\partial z_1}\frac{\partial G\left(\mathbf{R};\mathbf{r}_1,z_1\right)}{\partial z_1}\right]_{z_1=0}\eta\left(\mathbf{r}_1\right)\frac{d\mathbf{r}_1}{\rho}. \qquad (1)$$

Here integration is over the mean surface $z = 0$; $\mathbf{r}_1$ is a two-dimensional horizontal vector, $\mathbf{R}$ is a three-dimensional position vector; p_0 is the acoustic pressure in the monochromatic wave in the absence of surface roughness, i.e., in the "unperturbed" waveguide with the pressure-release boundary $z = 0$. Acoustic pressure in the full acoustic field in water equals $p_{sc} + p_0$; p_0 contains the incident wave and the wave reflected from the flat (horizontal) ocean surface. Surface elevation $\eta(\mathbf{r})$ is the vertical deviation of the rough surface from the mean plane $z = 0$. Mathematically, the rough surface is given by the equation $z = \eta(\mathbf{r})$. Note that $p_{sc} \to 0$ in the limit $\eta \to 0$ of vanishing roughness. In Eq. (1), $G(\mathbf{R}; \mathbf{R}_1)$ is the acoustic Green's function in the ocean with the flat upper boundary $z = 0$. The Green's function has the meaning of the acoustic pressure at point $\mathbf{R}$ due to a point sound source of volume velocity located at $\mathbf{R}_1$. In the water column, the Green's function satisfies the equation[55]

$$\frac{\partial}{\partial\mathbf{R}}\left[\frac{1}{\rho}\frac{\partial}{\partial\mathbf{R}}G\left(\mathbf{R};\mathbf{R}_1\right)\right]+\frac{\omega^2}{\rho c^2}G\left(\mathbf{R};\mathbf{R}_1\right)=-\delta\left(\mathbf{R}-\mathbf{R}_1\right) \qquad (2)$$

as well as the appropriate boundary conditions on the ocean surface and the seafloor. Here $\delta(\mathbf{R})$ is the Dirac delta function. The approximate solution Eq. (1) for the scattered wave describes single scattering from the rough surface but accounts for all multiple reflections in the ocean with the horizontal upper boundary.[53–55]

The physical meaning of Eq. (1) is that, in the first approximation of the small perturbation method, the waves scattered from the rough ocean surface are described as the waves generated by a known, distributed sound source in the ocean with the flat upper boundary. Indeed, acoustic pressure in the field generated by monochromatic sound sources in an inhomogeneous fluid satisfies the reduced wave equation[55]

$$\nabla\cdot\left(\frac{\nabla p}{\rho}\right)+\frac{\omega^2}{\rho c^2}p=i\omega A+\nabla\cdot\left(\frac{\mathbf{F}}{\rho}\right), \tag{3}$$

where **F** and *A* stand for the volume densities of the external force and volume velocity (i.e., the volume injection rate), respectively. In terms of the acoustic Green's function *G* of the medium, solution of the reduced wave equation is given by the equation[55]

$$p(\mathbf{R})=\int\left[\frac{\mathbf{F}(\mathbf{R}_1)}{\rho(\mathbf{R}_1)}\cdot\frac{\partial G(\mathbf{R};\mathbf{R}_1)}{\partial \mathbf{R}_1}-i\omega A(\mathbf{R}_1)G(\mathbf{R};\mathbf{R}_1)\right]d\mathbf{R}_1\,, \tag{4}$$

where the integration is over the entire volume occupied by the sources. Comparison of Eq. (1) and (4) shows that, in the first approximation of the small perturbation method, the scattered wave coincides with the field that would be generated in the medium with horizontal upper boundary by external forces with density

$$\mathbf{F}(\mathbf{r}_1,z_1)=\left(0,\quad 0,\quad -\eta(\mathbf{r}_1)\frac{\partial p_{in}}{\partial z_1}\delta(z_1)\right). \tag{5}$$

Equation (5) describes an effective vertical external force applied on the horizontal ocean surface. The effective sound source depends on the incident wave and the roughness of the actual ocean surface.

One can also reach the same conclusion that the scattered wave in an inhomogeneous medium is equivalent to the sound field generated by the effective sound source Eq. (5) on the horizontal boundary by comparing the boundary condition[53, 54]

$p_{sc}\left(\mathbf{r}_1, z=+0\right) = -\eta\left(\mathbf{r}_1\right)\left(\partial p_{in}/\partial z_1\right)_{z_1=0}$ for the scattered wave in the first approximation of the small perturbation method with the discontinuity (jump)[55] $p\left(\mathbf{r}_1, z=+0\right) - p\left(\mathbf{r}_1, z=0\right)$ $= p\left(\mathbf{r}_1, z=+0\right) = F_{0z}\left(\mathbf{r}_1\right)$ of the acoustic pressure, which, according to Eq. (3), is caused by the distribution of external vertical forces with volume density $F_{0z}\delta\left(z\right)$ just below a pressure-release boundary z = 0. Here z = +0 denotes points situated below the boundary z = 0 infinitesimally close to it.

B. Excitation of normal modes at surface scattering

In a horizontally stratified oceanic waveguide with a fluid seabed, the acoustic Green's function is given by the sum of normal modes[55, 56]

$$\begin{aligned} G\left(\mathbf{R};\mathbf{R}_1\right) &= \frac{i}{4}\sum_n f_n\left(z\right) f_n\left(z_1\right) H_0^{(1)}\left(\xi_n\left|\mathbf{r}-\mathbf{r}_1\right|\right) \\ &= \sum_n f_n\left(z\right) f_n\left(z_1\right) \frac{\exp\left(i\xi_n\left|\mathbf{r}-\mathbf{r}_1\right| + i\pi/4\right)}{\sqrt{8\pi\xi_n\left|\mathbf{r}-\mathbf{r}_1\right|}}\left[1 + O\left(\frac{1}{\xi_n\left|\mathbf{r}-\mathbf{r}_1\right|}\right)\right] \end{aligned} \qquad (6)$$

plus a contribution of the continuous spectrum. The latter is usually negligible at long-range propagation. Here $H_0^{(1)}(\cdot)$ is a Hankel function of the first kind of order zero, ξ_n and $f_n(z)$ are the propagation constant and shape function of the nth normal mode, n = 1, 2, …. The shape functions are normalized by the condition

$$\int_0^\infty \frac{dz}{\rho\left(z\right)} f_n^2\left(z\right) = 1. \qquad (7)$$

The shape function $f_n(z)$ gives the vertical dependence of acoustic pressure in the nth normal mode. When the horizontal separation of the points $\mathbf{R} = (\mathbf{r}, z)$ and $\mathbf{R}_1 = (\mathbf{r}_1, z_1)$ is large compared to the wavelength, the Hankel function can be replaced by the dominant term of its asymptotic expansion[57] leading to the right-most side in Eq. (6). With the points **R** and $\mathbf{R}_1$ located in water, Eq. (6) remains valid in the waveguide with stratified solid seabed[58] but, instead of Eq. (7), the normalization condition of the normal mode shape functions in the fluid-solid waveguide takes the form

$$\int_0^H \rho^{-1} f_n^2 dz + \frac{\omega}{\xi_n} \int_H^{+\infty} \left(\tau_{xz} v_z - \tau_{xx} v_x\right) \rho dz = 1, \tag{8}$$

where H is water depths, τ_{xx} and τ_{xz} are components of the stress tensor and v_x and v_z are components of the particle velocity $\mathbf{v} = (v_x, 0, v_z)$ in the seabed in the nth normal mode with the dependence $\exp(i\xi_n x)$ of its field on horizontal coordinates.[58] The shape functions $f_n(z)$ are real-valued in the absence of dissipation. The physical meaning of the normalization Eq. (8) is that modes with the same amplitude carry the same power flux; the acoustic power flux J_n in a single propagating normal mode with $p(\mathbf{r}, z) = af_n(z) H_0^{(1)}(\xi_n r)$, where a is a constant, equals $J_n = 2\left|a^2\right|/\omega$.[55, 56, 58]

Substitution of the Green's function Eq. (6) into Eq. (1) for the scattered wave and changing the order of the summation and integration gives

$$p_{sc}(\mathbf{r}, z) = \sum_n \frac{f_n(z) \exp(-3i\pi/4)}{\sqrt{8\pi\xi_n} \rho(0)} \left.\frac{\partial f_n}{\partial z}\right|_{z=0} Q_n(\mathbf{r}), \tag{9}$$

$$Q_n(\mathbf{r}) = \int d\mathbf{r}_1 \frac{\exp\left(i\xi_n |\mathbf{r} - \mathbf{r}_1|\right)}{\sqrt{|\mathbf{r} - \mathbf{r}_1|}} \eta(\mathbf{r}_1) \frac{\partial p_0}{\partial z_1}(\mathbf{r}_1, z_1 = 0), \tag{10}$$

provided $\xi_n |\mathbf{r} - \mathbf{r}_1| >> 1$. Equation (9) represents the scattered wave in the waveguide as a sum of normal modes, with $f_n(z)$ being the dependence of the acoustic pressure on depth in the nth normal mode. In the summand, the factor in front of Q_n is controlled by the waveguide's properties and the receiver depth. Dependence on horizontal coordinates of the receiver, the incident wave, and the properties of the rough surface is described by the factor Q_n, Eq. (10). When discussing the scattered wave, we will refer to Q_n as the mode amplitude for brevity.

Equations (9) and (10) show that each normal-mode component of p_{sc} is a result of interference of the contributions generated by scattering at different points on the rough surface. A more intuitive derivation of the normal-mode representation, Eqs. (9) and (10), of the scattered wave is obtained using the concept of the effective sources of the scattered wave. The surface density of the effective vertical force on the flat surface of a horizontally stratified oceanic waveguide is given by Eq. (5). A point source of the vertical force with $\mathbf{F}(\mathbf{r}_1, z_1) = (0,\ 0,\ F_0\delta(\mathbf{r}_1)\delta(z_1))$ generates the acoustic field[56]

$$p(\mathbf{R}) = \frac{iF_0}{4\rho(z_1)} \sum_n f_n(z) \frac{\partial f_n(z_1)}{\partial z_1} H_0^{(1)}\left(\xi_n |\mathbf{r} - \mathbf{r}_1|\right) \qquad (11)$$

in the waveguide. Here, as in Eq. (6) for the Green's function, we disregard the continuous spectrum of the field. Adding the contributions (11) of elementary effective sources located at different points on the boundary, i.e., by calculating the convolution of the field of a unit vertical force with the source density Eq. (5), leads again to Eqs. (9) and (10).

Equation (10) can be further simplified in the far field of the distributed effective source of the scattered wave. However, the far field assumption proves to be too restrictive to be useful in the *T*-phase excitation problem. For orientation, with the effective source dimensions of $L_T = O(10 \text{ km})$ and sound frequency $f \sim 20$ Hz the far-field condition $r >> \xi_n L_T^2$ requires the range r from the epicenter to be more than 10 Mm. Here, we will obtain more relevant and widely applicable results by taking into account that the correlation scale of the ocean surface roughness is much smaller than L_T.

As discussed in Sec. III C, extensive areas on the ocean surface can contribute to *T*-phase generation, and we need to allow for variations of the surface roughness statistics within these areas. Let the ocean surface elevation $\eta(\mathbf{r})$ have zero mean and be a locally stationary random function;[53] then $\langle \eta(\mathbf{r}) \rangle = 0$ and

$$\langle \eta(\mathbf{r}_1)\eta(\mathbf{r}_2) \rangle = C\left(\mathbf{r}_1 - \mathbf{r}_2; \frac{\mathbf{r}_1 + \mathbf{r}_2}{2}\right). \quad (12)$$

Here and below angular brackets $\langle \cdot \rangle$ denote statistical average; C has the meaning of the correlation function of the surface elevations. The characteristic spatial scales l and L of the variation of the correlation function with respect to the difference $\mathbf{r}_1 - \mathbf{r}_2$ and centroid $0.5(\mathbf{r}_1 + \mathbf{r}_2)$ coordinates satisfy the condition $l \ll L$. In the particular case of wide-sense stationary random elevations, $L \to \infty$ and the correlation function C depends only on $\mathbf{r}_1 - \mathbf{r}_2$. In terms of the correlation function, the root mean square (rms) surface elevation σ_η and the roughness spectrum are given by the equation $\sigma_\eta = \langle \eta^2(\mathbf{r}) \rangle^{1/2} = \sqrt{C(0;\mathbf{r})}$ and

$$S_\eta(\mathbf{q};\mathbf{r}) = (2\pi)^{-2} \int C(\mathbf{r}_1;\mathbf{r}) \exp(-i\mathbf{q}\cdot\mathbf{r}_1)\, d\mathbf{r}_1. \quad (13)$$

The spectrum and rms elevation of the surface roughness gradually vary with the position $\mathbf{r}$.

At reflection from the random rough surface, mode amplitudes Eq. (10) are also random, and $\langle Q_n(\mathbf{r}) \rangle = 0$. For the mode amplitude variance, from Eqs. (10) and (12) we find

$$\langle |Q_n^2(\mathbf{r})| \rangle = \int d\mathbf{r}_1 d\mathbf{r}_2 \frac{\exp\left[i\xi_n\left(|\mathbf{r}-\mathbf{r}_1| - |\mathbf{r}-\mathbf{r}_2|\right)\right]}{\sqrt{|\mathbf{r}-\mathbf{r}_1||\mathbf{r}-\mathbf{r}_2|}} C\left(\mathbf{r}_1 - \mathbf{r}_2; \frac{\mathbf{r}_1 + \mathbf{r}_2}{2}\right) \frac{\partial p_0(\mathbf{r}_1, 0)}{\partial z} \left(\frac{\partial p_0(\mathbf{r}_2, 0)}{\partial z}\right)^*. \quad (14)$$

Here and below the asterisk * denotes complex conjugation. The main contribution to the integral is from such $\mathbf{r}_1$ and $\mathbf{r}_2$ that $|\mathbf{r}_1 - \mathbf{r}_2|$ is of the order of or smaller than the roughness correlation scale l. When the horizontal separation r from the epicenter is large compared to the size L_T of the effective source of the scattered wave and $r >> \xi_n l^2$, one can approximate the product $|\mathbf{r} - \mathbf{r}_1|\,|\mathbf{r} - \mathbf{r}_2|$ with r^2 in the integrand in Eq. (14) and retain in the exponent only linear terms of the developments

$$\left|\mathbf{r}-\frac{\mathbf{r}_1+\mathbf{r}_2}{2}\pm\frac{\mathbf{r}_1-\mathbf{r}_2}{2}\right|=\left|\mathbf{r}-\frac{\mathbf{r}_1+\mathbf{r}_2}{2}\right|\pm\left|\mathbf{r}-\frac{\mathbf{r}_1+\mathbf{r}_2}{2}\right|^{-1}\left(\mathbf{r}-\frac{\mathbf{r}_1+\mathbf{r}_2}{2}\right)\cdot\frac{\mathbf{r}_1-\mathbf{r}_2}{2}+O\left(\frac{|\mathbf{r}_1-\mathbf{r}_2|^2}{|2\mathbf{r}-\mathbf{r}_1-\mathbf{r}_2|^2}\right) \quad (15)$$

of $|\mathbf{r} - \mathbf{r}_j|$, $j = 1, 2$, in powers of $|\mathbf{r}_1 - \mathbf{r}_2|$. We also assume that the unperturbed field p_0 can be represented as

$$p_0(\mathbf{r},z)=P(\mathbf{r},z)\exp\left[i\mathbf{q}_{in}(\mathbf{r})\cdot\mathbf{r}\right] \quad (16)$$

in the vicinity of the ocean surface in water. Here the complex amplitude P and the local horizontal wave vector $\mathbf{q}_{in}$ are gradually varying functions of $\mathbf{r}$, which are little changed over distances $O(l)$.

Changing integration variables in Eq, (14) from $\mathbf{r}_1$ and $\mathbf{r}_2$ to the difference and centroid position vectors, $\mathbf{r}_1 - \mathbf{r}_2$ and $\mathbf{r}_3 = 0.5(\mathbf{r}_1 + \mathbf{r}_2)$, and using Eqs. (13), (15), and (16), we obtain a compact expression for the mode amplitude variance:

$$\left\langle\left|Q_n^2(\mathbf{r})\right|\right\rangle=\frac{4\pi^2}{r}\int d\mathbf{r}_3\left|\frac{\partial P(\mathbf{r}_3,0)}{\partial z}\right|^2 S_\eta\left(\xi_n\mathbf{e}-\mathbf{q}_{in};\mathbf{r}_3\right),\quad \mathbf{e}=\frac{\mathbf{r}-\mathbf{r}_3}{|\mathbf{r}-\mathbf{r}_3|}. \quad (17)$$

Here $\mathbf{e}$ has the meaning of the unit horizontal vector from an elementary scatterer to the observation point, and $\xi_n\mathbf{e}$ is the horizontal wave vector of the nth mode propagating from $\mathbf{r}_3$ to $\mathbf{r}$. For the distant observation points that we consider, it is close to the unit horizontal vector from the epicenter to the observation point: $\mathbf{e}=r^{-1}\mathbf{r}+O(L_T/r)$. Inspection shows that Eq. (17) is consistent with the more general result, Eq. (9) in Ref. 59, for the cross-correlation function of the surface reverberation in the oceanic waveguide.

Integration in Eq. (17) is over the entire horizontal plane $z = 0$. The ocean surface area that significantly contributes to normal mode excitation is controlled by the decrease of the amplitude of the unperturbed field p_0 with horizontal separation from the epicenter and is affected by spatial distribution of the surface roughness. The integrand is proportional to the average power scattered into the nth mode in the vicinity of the point $(\mathbf{r}_3, 0)$ on the ocean surface. The contributions of different points into the average mode's power are added incoherently, according to Eq. (17). The first argument, $\xi_n\mathbf{e} - \mathbf{q}_{in}$, of the roughness spectrum S_η in the integrand equals the change of the horizontal wave vector of sound at scattering and corresponds to Bragg's scattering, as expected in the first approximation of the small perturbation method.[53, 54] We will use Eq. (17) in Section III to investigate the effects on T-phase generation of the wind speed, sea swell parameters, and depth of the earthquake focus.

Acoustic power flux in T waves can be calculated by integrating the power flux density over the cylindrical surface $r = \text{const.} > L_T$, $0 < z < \infty$. At distances r from the epicenter that are large compared to the diameter L_T of the region, where T waves are excited , $\nabla Q_n \approx i\xi_n r^{-1} Q_n \mathbf{r}$ according to Eq. (10). Using this equation and the normalization condition (8), for the power flux J_n in the nth mode we find

$$J_n = \frac{r}{16\pi\omega}\left(\frac{1}{\rho}\frac{\partial f_n}{\partial z}\right)^2_{z=0} \int_0^{2\pi} \left| Q_n^2\left(r\cos\varphi, r\cos\varphi\right)\right| d\varphi \tag{18}$$

from Eq. (9). The total power flux is given by the sum of the contributions J_n, Eq. (18), of all propagating normal modes. For a random rough surface with the spectrum S_η, Eqs. (17) and (18) give

$$\langle J_n \rangle = \frac{\pi}{4\omega}\left(\frac{1}{\rho}\frac{\partial f_n}{\partial z}\right)^2_{z=0} \int_0^{2\pi} \left[\int d\mathbf{r}_3 \left| \frac{\partial P(\mathbf{r}_3, 0)}{\partial z} \right|^2 S_\eta\left(\xi_n \mathbf{e} - \mathbf{q}_{in}; \mathbf{r}_3\right) \right] d\varphi, \tag{19}$$

where $\mathbf{e} = (\cos\varphi, \sin\varphi, 0)$. As expected, the power flux is independent of r as long as the effect of absorption on the propagating normal mode is negligible over ranges of the order of r.

C. Excitation of normal modes at volume scattering by internal gravity waves

Consider internal gravity waves propagating in otherwise horizontally stratified, stationary ocean. The internal wave-induced currents $\mathbf{u}$ and variations of the sound speed, δc, and density, $\delta\rho$, from their unperturbed (background) values $c(z)$ and $\rho(z)$ are horizontally inhomogeneous. The currents are slow and environmental perturbations are weak in the following sense: $|\delta c| + u << c$, $\delta\rho << \rho$. Neglecting terms of the second order in the small ratio u/c, monochromatic acoustic waves satisfy the following wave equation[55, 60] in the horizontally inhomogeneous ocean with slow currents:

$$\nabla\cdot\left(\frac{\nabla p}{\rho_0}\right)+\frac{\omega^2}{\rho_0 c_0^2}p+\frac{2i\omega}{\rho_0 c_0^2}\mathbf{u}\cdot\nabla p-\frac{2i}{\omega}\nabla\cdot\left(\frac{1}{\rho_0}\sum_{j=1}^{3}\frac{\partial p}{\partial x_j}\frac{\partial \mathbf{u}}{\partial x_j}\right)=0. \qquad (20)$$

Here $\rho_0 = \rho + \delta\rho$, $c_0 = c + \delta c$, and $(x_1, x_2, x_3) = (x, y, z)$ are Cartesian coordinates. Acoustic pressure $p = p_0 + p_{sc}$ consists of the acoustic pressure p_0 in the horizontally stratified ocean and the perturbation (scattered wave) p_{sc}. In the water column, p_0 satisfies Eq. (20) with $\mathbf{u} = 0$ and ρ_0 and c_0 replaced with ρ and c, respectively.

The scattered wave vanishes when the environmental perturbations $\mathbf{u}$, δc, and $\delta\rho$ vanish. Retaining only terms of the first order in the acoustic and environmental perturbations, from Eq. (20) we find

$$\nabla\cdot\left(\frac{\nabla p_{sc}}{\rho}\right)+\frac{\omega^2}{\rho c^2}p_{sc}=i\omega A_{sc}+\nabla\cdot\left(\frac{\mathbf{F}_{sc}}{\rho}\right), \qquad (21)$$

where

$$A_{sc} = \frac{-i\omega p_0}{\rho c^2}\left(\frac{\delta\rho}{\rho}+\frac{2\delta c}{c}\right)-\frac{2}{\rho c^2}\mathbf{u}\cdot\nabla p_0, \quad \mathbf{F}_{sc} = \frac{\delta\rho}{\rho}\nabla p_0 + \frac{2i}{\omega}\sum_{j=1}^{3}\frac{\partial p_0}{\partial x_j}\frac{\partial \mathbf{u}}{\partial x_j}. \qquad (22)$$

The above assumptions correspond to calculation of the scattered wave in the single-scattering, or (first) Born, approximation. Comparison of Eqs. (3) and (21) shows, that in the Born approximation the scattered wave can be viewed as the wave generated in horizontally stratified ocean by distributed virtual sources with volume densities A_{sc} and $\mathbf{F}_{\mathrm{sc}}$, Eq. (22), respectively, of the volume velocity and external force. Using Eq. (4) for the field of distributed sources and Eq. (6) for the Green's function, we find the scattered wave in the following form:

$$p_{sc}(\mathbf{r},z) = \sum_n \frac{f_n(z)\exp(-i\pi/4)}{\sqrt{8\pi\xi_n}} V_n(\mathbf{r}), \qquad (23)$$

where

$$V_n(\mathbf{r}) = \int d\mathbf{r}_1 \frac{\exp(i\xi_n|\mathbf{r}-\mathbf{r}_1|)}{\sqrt{|\mathbf{r}-\mathbf{r}_1|}} \int \frac{dz_1}{\rho}\left[\left(\omega\rho A_{sc} + \xi_n \frac{\mathbf{r}-\mathbf{r}_1}{|\mathbf{r}-\mathbf{r}_1|}\cdot\mathbf{F}_{sc}\right) f_n + i\frac{\partial f_n}{\partial z_1}(\mathbf{F}_{sc})_z\right], \qquad (24)$$

and $(\mathbf{F}_{sc})_z$ stands for the vertical component of the vector $\mathbf{F}_{sc}$ defined in Eq. (22). Equation (23) represents the scattered wave as a sum of normal modes, with V_n describing the dependence of the nth mode amplitude on horizontal coordinates.

In small-amplitude, or linear, internal waves, the sound speed and density perturbations are proportional to the vertical displacement ζ of fluid particles due to the internal wave: $\delta c = \alpha_1(z)c\zeta$, $\delta\rho = \alpha_2(z)\rho\zeta$.[46] Vertical velocity u_3 of fluid particles is given by time derivative of ζ, and horizontal components of the velocity are related to ζ by the incompressibility condition $\nabla\cdot\mathbf{u} = 0$.[46] In a random field of linear internal waves, let the vertical displacement ζ have zero mean and be a random function that is locally stationary in the horizontal plane. Then the correlation function of vertical displacements is related to the spatial spectrum S_ζ of internal waves as follows:

$$\left\langle \zeta\left(\mathbf{r}_1, z_1\right)\zeta\left(\mathbf{r}_2, z_2\right)\right\rangle = \int S_\zeta\left(\mathbf{q}; z_1, z_2; \frac{\mathbf{r}_1+\mathbf{r}_2}{2}\right) e^{i\mathbf{q}\cdot(\mathbf{r}_1-\mathbf{r}_2)} d\mathbf{q}, \tag{25}$$

Under these assumptions, the densities of the effective sources of the scattered sound wave are also zero-mean random functions that are locally stationary in the horizontal plane. Using Eq. (22), the spectra of the random sources can be related to the spectrum of the vertical displacement of fluid particles; importantly, the source spectra have the same spatial scales as S_ζ.

At scattering by random internal waves, the mode amplitudes V_n are random and have zero mean. Calculation of the variance of the mode amplitude, and particularly the reduction of a double integral over horizontal coordinate to a single integral, is similar to the calculation of $\left\langle \left| Q_n^2 \right| \right\rangle$ in Sec. II B. From Eqs. (16), (22), (24), and (25) we find that

$$\begin{gathered} \left\langle \left| V_m^2(\mathbf{r}) \right| \right\rangle = \frac{4\pi^2}{r} \int d\mathbf{r}_3 dz_1 dz_2 \Phi\left(\mathbf{r}_3, z_1\right) \Phi\left(\mathbf{r}_3, z_2\right)^* S_\zeta\left(\xi_m \mathbf{e} - \mathbf{q}_{in}; z_1, z_2; \mathbf{r}_3\right), \\ \Phi(\mathbf{r}, z) = \left[\alpha_2 \xi_m \mathbf{e}\cdot\mathbf{q}_{in} - k^2\left(2\alpha_1+\alpha_2\right)\right] \frac{f_m P}{\rho} + \frac{\alpha_2}{\rho} \frac{\partial P}{\partial z} \frac{\partial f_m}{\partial z}. \end{gathered} \tag{26}$$

Here, the unit horizontal vector **e** is the same as in Eq. (17). For brevity, contributions of the internal wave-induced currents into sound scattering are not included in Eq. (26). Equations (17) and (26), which describe the variances of mode amplitudes that are proportional to the power flux in respective normal modes resulting, respectively, from surface and volume scattering, differ by additional integration over depths z_1 and z_2 of volume scatterers in Eq. (26). Note that the spatial spectra S_η and S_ζ of the surface elevation and the vertical displacement due to internal waves in Eqs. (17) and (26) have the same vector argument $\xi_n \mathbf{e} - \mathbf{q}_{in}$, which equals the difference of the horizontal wave vectors of the normal mode and the incident wave.

Because of the large values of the compressional and shear wave speeds around the earthquake focus, earthquake-generated incident waves propagate at steep grazing angles in the water column, see Sec. III C for details. Therefore, $|\xi_n \mathbf{e} - \mathbf{q}_{in}| \sim \xi_n$. The internal wave spectrum peaks around 5 km horizontal wavelength, with minimum and maximum internal wave wavelength in the ocean being about 0.5 km and 50 km, respectively.[46] In the 3–50 Hz frequency range of observed *T* waves, horizontal wavelength $2\pi/\xi_n$ of acoustic normal modes ranges from about 30–500 m. Hence, the internal wave spectrum in the integrand in Eq. (26) has negligibly small values. The short-wave tail of the internal wave spectrum can possibly contribute to generation of the lowest-frequency *T* waves away from the earthquake epicenter. In other words, the internal wave field lacks the relatively short horizontal scales (< 500 m) that are required for Bragg scattering of the earthquake-generated body waves into normal modes of the underwater waveguide. As discussed below, ocean surface roughness spectrum is rich in the spatial scales required for Bragg scattering into normal modes and, therefore, efficiently contributes to *T*-phase generation.

III. CONTRIBUTIONS OF WIND SEAS AND SEA SWELL INTO *T*-PHASE GENERATION

A. *T*-phase excitation due to wind seas

Dependence of the ocean surface roughness on wind speed and fetch have been studied extensively, which allows for a reliable prediction of *T* waves generation at scattering by sea surface roughness. Here, we use a simple Pierson-Moskovitz model[43, 44] of fully developed wind seas to investigate the dependence of amplitudes of the normal mode components of the scattered acoustic wave on its frequency, wind speed, and direction of propagation of the incident wave.

The Pierson-Moskovitz spectrum[43, 44] of the random surface elevation η is given by the following equations:

$$S_\eta(\mathbf{q};\mathbf{r}) = W(q) D_W(q,\psi), \quad \int_{-\pi}^{\pi} D_W(q,\psi)\, d\psi = 1, \tag{27}$$

$$W(q) = \frac{0.024}{q^4} \exp\left(-\frac{0.74 g^2}{q^2 U^4} \right). \tag{28}$$

Here g is the acceleration due to gravity; U is the wind speed measured at height of 19.5 m above the sea surface. The factor D_W describes the directionality of the surface waves; $\mathbf{q} = q$ (cosψ, sinψ, 0) is the wave vector of the waves, and angle ψ indicates the vector **q** direction. The wind speed may gradually change along the ocean surface: $U = U(\mathbf{r})$, and W and D_W in Eqs. (27) and (28) depend on **r** via U. In wind waves with the Pierson-Moskovitz spectrum, the spectral peak is located at $q_p = 0.70 g U^{-2}$; and rms surface elevation $\sigma_\eta = 0.13 U^2 / g$. The wave height rapidly increases, and the spectrum peak shifts towards longer waves, when the wind speed increases (Fig. 2a). According to Eq. (28), the spectrum falls off very rapidly (exponentially) as the surface wave wavelength becomes longer than at the spectrum peak, i.e., at $q < q_p$. The spectrum decrease is much slower for short gravity waves, i.e., at $q > q_p$ (Fig. 2a). Because of the Bragg scattering condition, these properties of the wind wave spectrum are directly reflected in the spectrum of abyssal *T*-waves and its wind dependence.

The rms amplitude $\left\langle \left| Q_n^2 \right| \right\rangle^{1/2}$ of the nth normal mode component of the *T*-phase field is given by Eq. (17). Figure 2b illustrates the wind dependence of the *T*-phase energy in terms of the contribution to the acoustic power flux in a normal mode from a unit area of the sea surface above the earthquake focus. In this geometry, the horizontal wave vector of the incident wave $\mathbf{q}_{in} = 0$ in the right side of Eq. (17). Then, directionality of the *T*-phase radiation is given by the factor D_W in the wind wave spectrum Eq. (27). Equation (18) shows that the wind speed dependence of the acoustic power flux in the *T*-wave is obtained by integrating (or averaging) of $\left| Q_n^2 \right|$ over the *T*-wave propagation direction. In Fig. 2b we show the mode amplitude squared,

$\left|Q_n^2\right|$, that is averaged over the statistical ensemble of fully developed wind waves. It is also averaged over the *T*-wave propagation direction for a given wind direction or, equivalently, over the wind direction for a given receiver position. On the other hand, it follows from Eq. (27) that, after averaging over the wind direction, $\left\langle\left|Q_n^2\right|\right\rangle$ is given by Eq. (17), where $S_\eta\left(\xi_n\mathbf{e}-\mathbf{q}_{in};\mathbf{r}_3\right)$ is replaced with $W\left(\left|\xi_n\mathbf{e}-\mathbf{q}_{in}\right|\right)$ in the integrand. Hence, the result is independent of the surface wave directionality D_W and its dependence on q in Eq. (27). Since averaging over wind direction is equivalent to integration over receiver azimuth, acoustic power flux in *T*-waves is also independent of D_W at normal incidence of ballistic waves. Numerical values of the sound frequency f indicated in Fig. 2b refer to the mode with the nominal phase speed c_n of 1500 m/s. For a generic mode dispersion relation $c_n = c_n(f)$, the frequency f should be re-scaled to (1500 m/s)$f/c_n(f)$.

T-phase amplitude rapidly increases with the wind speed for weak and moderate winds and saturates at very high wind speeds (Fig. 2b). Higher acoustic frequencies are more readily excited by weaker winds and saturate at smaller wind speeds. For an incident wave with a white spectrum, higher acoustic frequencies dominate in the *T*-phase spectrum at low wind speeds, while low frequencies prevail at strong winds. Abyssal *T*-phase energy and spectrum can be very sensitive to the wind speed. Away from the saturation regime, a drastic, 40 dB increase in the narrow-band mode amplitude requires an increase in the wind speed of just a few meters per second (Fig. 2b).

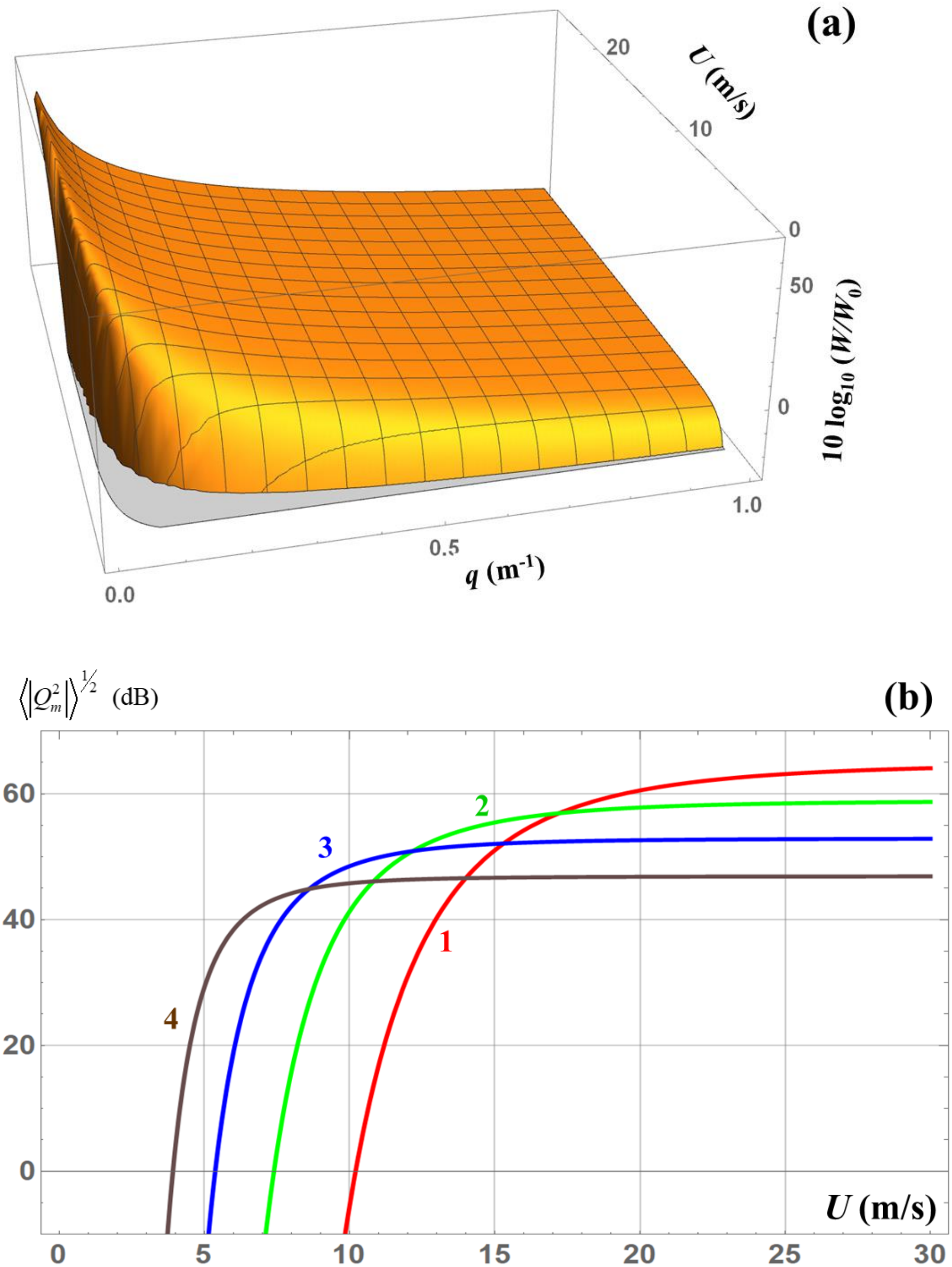

Figure 2. (Color online) Dependence of the abyssal *T*-phase mode amplitude on wind speed. (a) Azimuthally averaged Pierson-Moskovitz spectrum of wind waves as described by Eq. (28) is shown as a function of surface gravity wave wavenumber *q* and wind speed *U* at 19.5 m above

the sea surface; $W_0 = 1$ m^4. (b) The rms amplitude of a normal mode of the *T*-waves generated by scattering on wind seas in a unit area above the earthquake focus is shown for four frequencies: 5 Hz (1), 10 Hz (2), 20 Hz (3) and 40 Hz (4), and the mode phase speed of 1500 m/s. The mode amplitude is arbitrarily normalized assuming a frequency-independent acoustic pressure amplitude in the earthquake-generated incident wave.

The spectrum of *T*-waves at different wind speeds is further illustrated in Fig. 3. The figure shows the mode amplitude squared, $\left|Q_n^2\right|$, which is averaged over the statistical ensemble of fully developed wind waves and over the wind direction. Therefore, the result is independent of the wind waves directionality that is described by the factor $D_W(q, \psi)$ in Eq. (27). Similar to Fig. 2b, Fig. 3a refers to the *T*-phase generation at normal incidence of ballistic waves from the earthquake focus. The figure shows a steady increase of normal mode amplitudes with wind speed in the entire range of *T*-phase frequencies. The most distinctive feature of the predicted *T*-phase spectra is a sharp low-frequency cutoff. At low acoustic frequencies, Bragg scattering into proper normal modes of the underwater waveguide requires long wind waves, with their wavevector matching the horizontal wave vector of the acoustic normal mode, see Eq. (17). For instance, the resonance scattering into the modes at 5 Hz occurs at surface gravity waves with wavelength of about 300 m. Thus, the low-frequency acoustic cutoff reflects the sharp drop in the wind wave spectrum at $q < q_p$. The cutoff shifts to lower acoustic frequencies and the *T*-phase spectrum broadens when the wind speed increases (Fig. 3a).

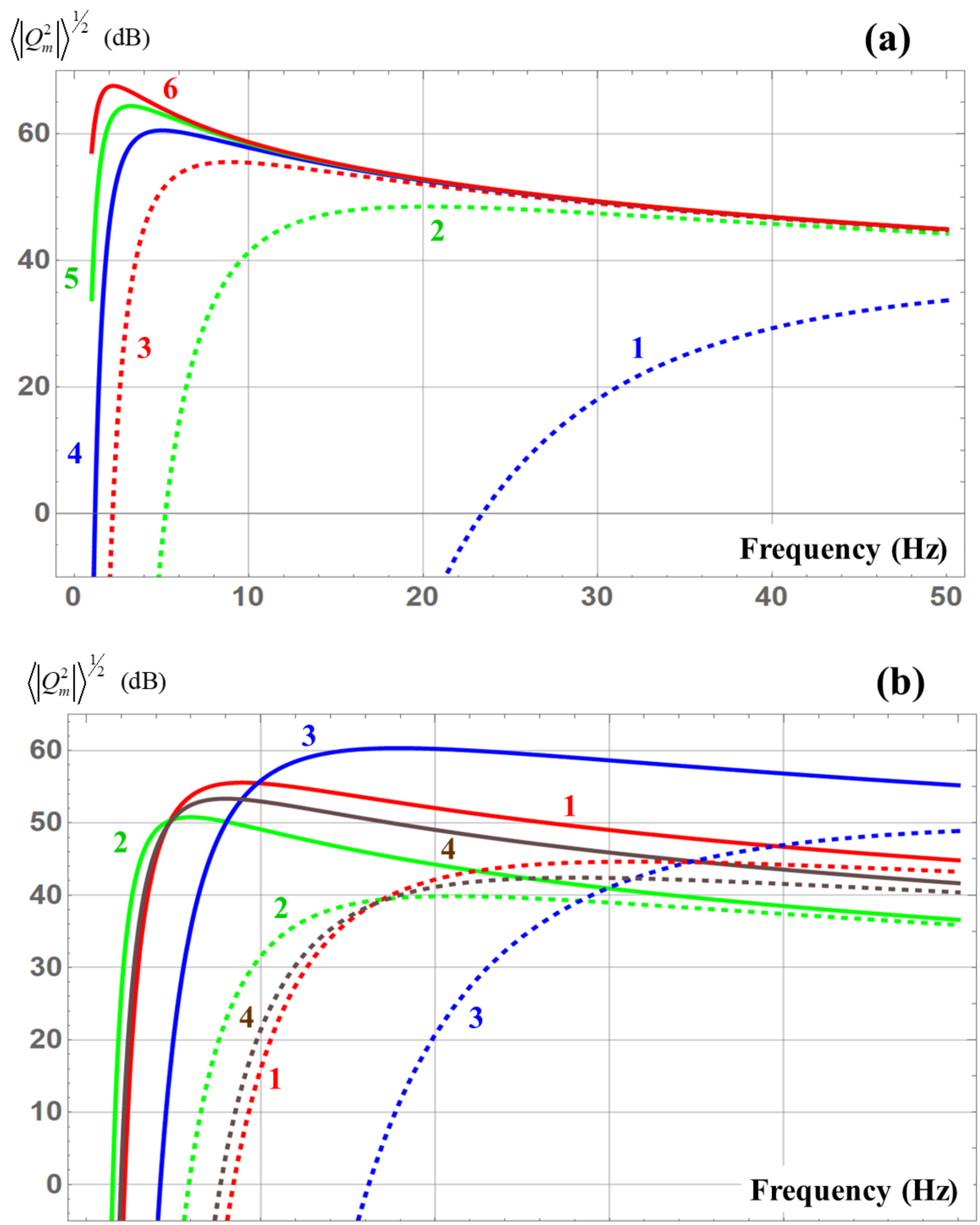

Figure 3. (Color online) Dependence of the amplitude of a modal component of the *T*-wave, which is generated by scattering on fully developed wind seas, on sound frequency and the mode propagation direction. (a) The frequency dependences of the rms amplitude of a normal mode,

which is generated by scattering in a unit area above the earthquake focus, are shown for six wind speeds: 5 m/s (1), 10 m/s (2), 15 m/s (3), 20 m/s (4), 25 m/s (5) and 30 m/s (6). (b) The rms amplitude of a normal mode is shown for scattering in a unit area above the earthquake focus (1) and away from the epicenter (2–4), where the grazing angle of the earthquake-generated incident wave is 60° at the depth, where $c(z) = c_m$. The horizontal propagation directions of the mode and incident wave are either opposite (2), the same (3), or orthogonal (4). Solid and dashed lines refer to the wind speeds of 15 m/s and 8 m/s, respectively. A nominal value of 1500 m/s is assumed for the mode phase speed c_m.

The frequency dependence of the efficiency of *T*-wave generation by scattering of obliquely incident waves is qualitatively similar to but quantitatively different from the case of normal incidence. This is illustrated in Fig. 3b. At points on the ocean surface away from the earthquake epicenter, *T*-phase is generated with different amplitudes in different horizontal propagation directions, even after averaging over the wind direction (Fig. 3b). For obliquely incident waves, wind waves of different wavelength are responsible for the *T*-waves propagating in different azimuthal directions, see Eq. (17). When the incident wave and *T*-wave propagate in opposite horizontal directions, the low-frequency cutoff shifts somewhat towards lower frequencies; when the propagation directions are the same, there is a more significant shift towards higher frequencies (Fig. 3b).

In addition to the frequency dependence of the generation efficiency of each normal mode that is illustrated in Fig. 3, *T*-phase spectrum at a distant receiver is influenced by the number of propagating modes, which increases with frequency, frequency-dependent transmission losses due to sound attenuation, and the spectrum of the seismic source.

B. *T*-phase excitation due to swell

Statistically, wave height and surface gravity wave energy are dominated by sea swell, rather than wind waves, almost everywhere in the World Ocean.[45] We argue below that swell is also expected to dominate in generation of abyssal *T*-waves.

Sea swell is generated by very strong winds in distant storms. Because of the pronounced dispersion of surface gravity waves in deep water, swell is observed at large distances from its source as a wave train of long gravity waves with nearly identical wavelengths. A typical width of the wavetrain is several tens of wavelengths across the wavefronts with even longer extent along the wavefronts.[61] Thus, ocean surface elevations due to swell have much larger correlation length then the surface roughness caused by wind waves. This difference has a major effect on scattering of low-frequency sound. While wind waves can be modeled as a random wave field, it is more appropriate to model a snapshot of sea swell in an area of several and perhaps a few tens of km as a deterministic wave field.

Unlike wind waves, there are no widely accepted swell models. We will utilize the following simple, idealized model to illustrate distinctive features of *T*-phase generation at sound scattering by swell. At the time of an earthquake, let the surface elevation η in a swell wave train be

$$\eta(x,y)=\sqrt{2}\sigma_\eta(y)\sin(\mu x-\mu x_0), \quad |x-x_0|<L/2, \tag{29}$$

in a region of width L in the direction of swell propagation, which is chosen as the x coordinate axis; $\eta = 0$ at $|x - x_0| \geq L/2$. A large, integer number of swell wavelengths $2\pi/\mu$ fits in the band $|x-x_0| \leq L/2$, and $\eta(x, y)$ is a continuous function of horizontal coordinates. The rms surface elevation σ_η is a gradually varying function of y and tends to zero at $|y - y_0|\to\infty$, so that the energy of the wavetrain is finite. The center of the swell wavetrain is at the point (x_0, y_0, 0), which can be located either at the earthquake epicenter (0, 0, 0) or away from it.

At scattering of ballistic sound waves [Eq. (16)] at the ocean surface with surface elevations Eq. (29), Eq. (10) for the amplitude of a T-phase modal component becomes

$$Q_n(\mathbf{r}) = \sqrt{2}\int_{x_0-L/2}^{x_0+L/2} dx_1 \sin(\mu x_1 - \mu x_0) \int_{-\infty}^{\infty} dy_1 \frac{\exp\left(i\xi_n|\mathbf{r}-\mathbf{r}_1| + i\mathbf{q}_{in}\cdot\mathbf{r}_1\right)}{\sqrt{|\mathbf{r}-\mathbf{r}_1|}} \sigma_\eta(y_1) \frac{\partial P(\mathbf{r}_1, 0)}{\partial z}, \quad (30)$$

where the two-dimensional horizontal position vector $\mathbf{r}_1 = (x_1, y_1)$. In the integral over y_1 in Eq. (30), the integrand contains a rapidly varying exponential and slowly varying functions σ_η, $\mathbf{q}_{in} = (q_{in1}, q_{in2}, 0)$, and $\partial P/\partial z$. The integral can be calculated by the method of stationary phase.[55] Disregarding small derivatives of q_{in2}, equation for the stationary point[55] $y_1 = y_{1s}$ becomes

$$\frac{y - y_{1s}}{\sqrt{(x-x_1)^2 + (y-y_{1s})^2}} = \frac{q_{in2}}{\xi_n}. \quad (31)$$

For any observation point at $|x - x_0| > L/2$, the integrand has a single stationary point. By approximating the integral over y_1 in Eq. (30) by contribution of the stationary point,[55] we obtain

$$Q_n(\mathbf{r}) = 2\sqrt{\pi\xi_n}\, e^{i\pi/4} \times \int_{x_0-L/2}^{x_0+L/2} \frac{\sin(\mu x_1 - \mu x_0)\sigma_\eta(y_{1s})}{\sqrt{\xi_n^2 - q_{in2}^2}} \frac{\partial P(x_1, y_{1s}, 0)}{\partial z} \exp\left(i\sqrt{\xi_n^2 - q_{in2}^2}\,|x - x_1| + iq_{in1}x_1 + iq_{in2}y\right) dx_1. \quad (32)$$

Assuming negligible variation of σ_η, $\mathbf{q}_{in}$, and $\partial P/\partial z$ with x_1 within the swell wave train, the integral in the right side of Eq. (32) is easily calculated, and we obtain

$$Q_n(\mathbf{r}) = 2e^{i\pi/4}\sqrt{\frac{\pi\xi_n}{\xi_n^2 - q_{in2}^2}} \frac{\partial P}{\partial z} \sigma_\eta L \left(\frac{\sin Y_2}{Y_2} - \frac{\sin Y_1}{Y_1}\right) \exp\left(i\sqrt{\xi_n^2 - q_{in2}^2}\,|x - x_0| + iq_{in2}y\right), \quad (33)$$

where

$$Y_j = \left[q_{in1} - \sqrt{\xi_n^2 - q_{in2}^2}\,\frac{x - x_0}{|x - x_0|} + (-1)^j \mu\right]\frac{L}{2}, \quad j = 1,\ 2. \quad (34)$$

Equations (33) and (34) give the normal mode amplitudes in the abyssal *T* waves due to swell at the observation points at $|x - x_0| > L/2$, i.e., outside of the swell wavetrain.

The Bragg scattering condition and the narrow-band, quasi-periodic nature of surface elevation in swell wavetrains combine to produce rather different dependence of *T*-phase energy on the mode frequency and propagation direction than in the case of wind waves (cf. Figs. 2b and 3 with Fig. 4). Figure 4 illustrates predictions of Eqs. (33) and (34). At a given sound frequency and normal mode propagation direction, a swell wavetrain most efficiently generates *m*th normal mode at a specific grazing angle χ of the ballistic wave (Fig. 4a), with secondary peaks in χ giving *T* waves that are weaker by tens of dB (Fig. 4a). The contrast between the main and subsequent peaks is controlled by the parameter $\mu L \gg 1$. The resonance value of the grazing angle χ depends on the wavetrain position relative to the epicenter via the angle between azimuthal directions of the swell and ballistic wave propagation (Fig. 4a). For the sound frequency and swell wavelength (10 Hz and 200 m) in Fig. 4a, resonance excitation occurs for the wavetrains away from the epicenter, where χ is between about 47° and 78°.

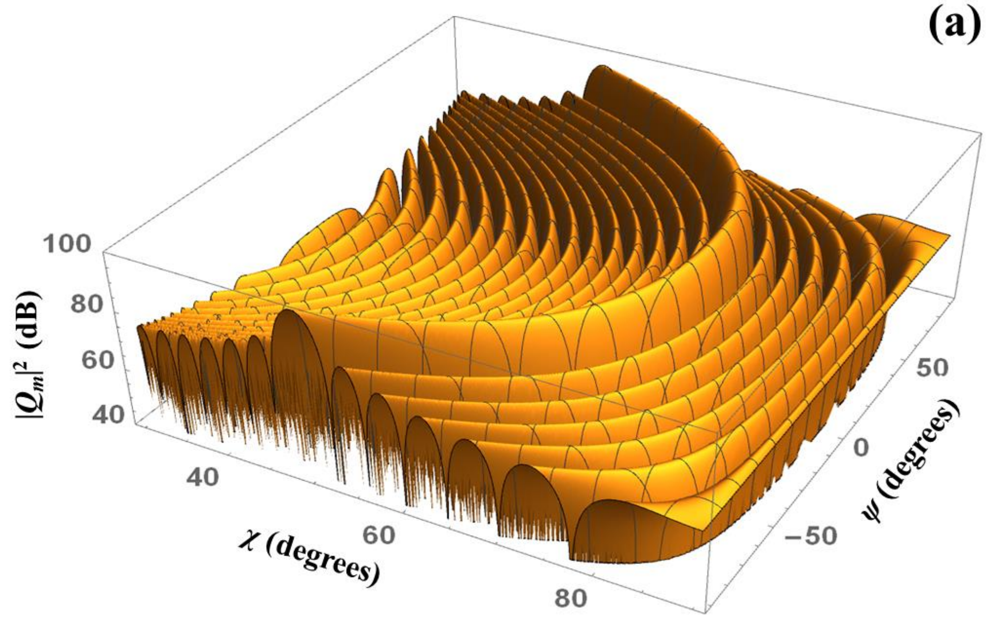
(a)
100
80
60
40
$|Q_m|^2$ (dB)
40
60
80
χ (degrees)
50
0
−50
ψ (degrees)

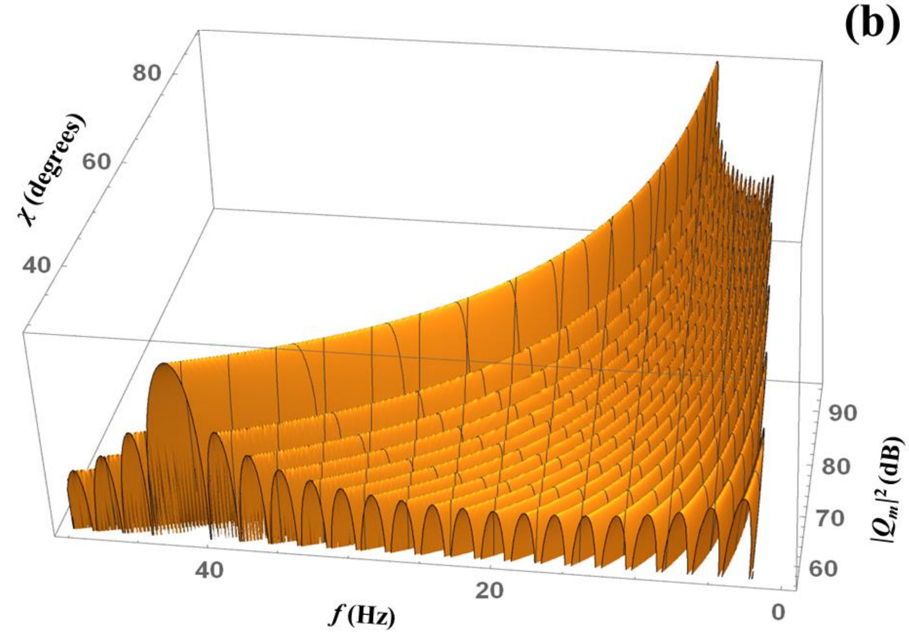
(b)
80
60
40
χ (degrees)
90
80
70
60
$|Q_m|^2$ (dB)
40
20
0
f (Hz)

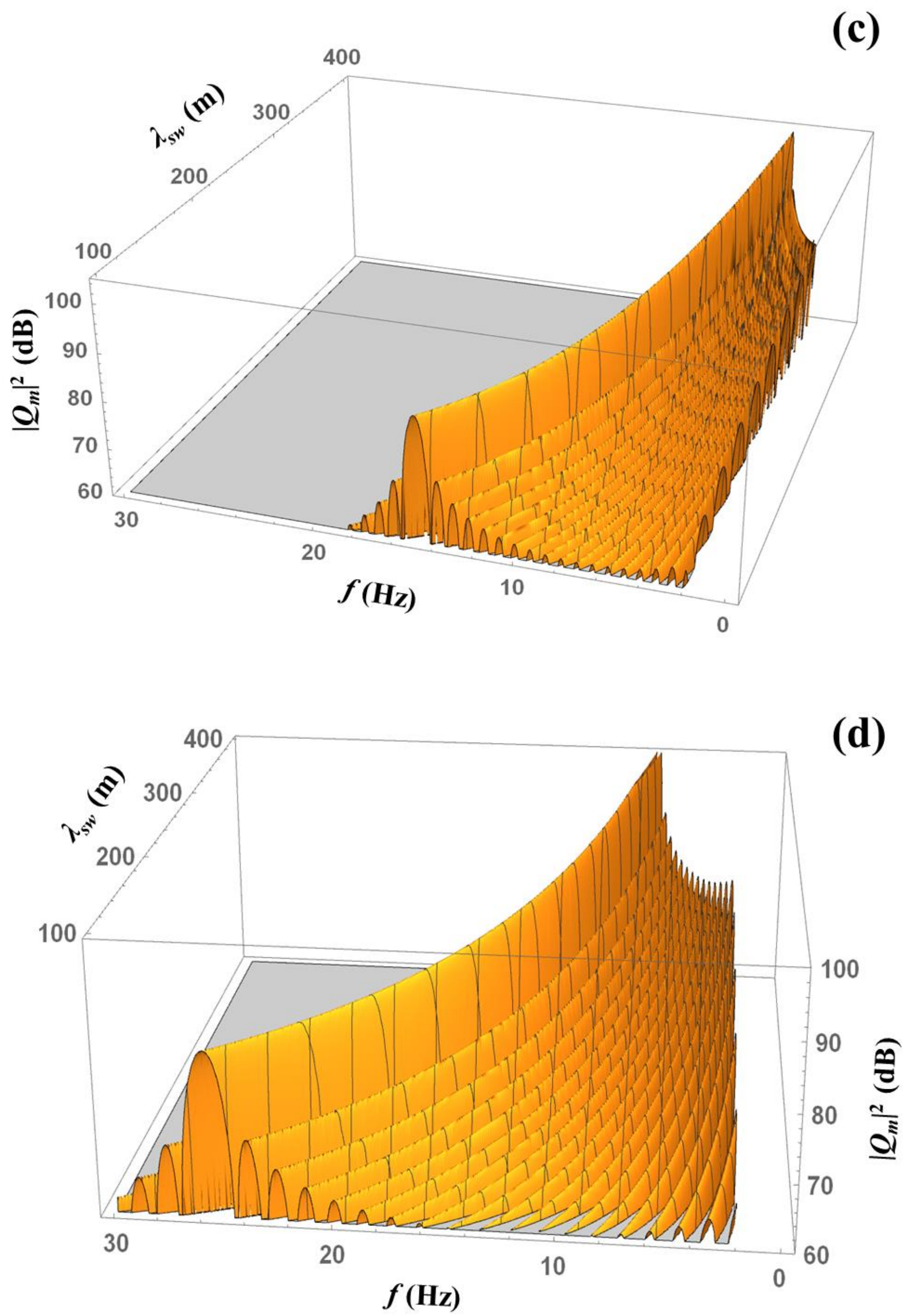

Figure 4. (Color online) Generation of *T* waves at scattering of ballistic waves from an earthquake by a wavetrain of sea swell. (a) Dependence of the amplitude of a normal-mode component of the *T* wave on the grazing angle χ of incident wave at the location of the swell

wavetrain and the angle ψ between the azimuthal directions of propagation of the incidence waves and swell. Sound frequency is 10 Hz. Swell wavelength λ_{sw} = 200 m. (b) Variation of the normal mode amplitude with the grazing angle of incident waves and sound frequency, when the angle between the azimuthal directions of propagation of the incidence waves and swell is 45°. Swell wavelength λ_{sw} = 200 m. (c) Dependence of the acoustic mode amplitude on sound frequency and the wavelength of swell at normal incidence for vertically propagating ballistic waves. (d) Same as in (c) but for the swell wavetrain located away from the earthquake epicenter; χ = 60°, ψ = 45°. A common but otherwise arbitrary normalization of the acoustic mode amplitude is used in all panels. The width of the swell wavetrain in the direction of its propagation equals 20 swell wavelengths. A nominal value of 1500 m/s is assumed for the phase speed c_m of the acoustic normal mode. Numerical values of the grazing angle of the earthquake-generated incident waves refer to the depth, where $c(z) = c_m$.

T-phase spectrum and, in particular, the frequency, at which a normal mode is resonantly generated, depend on the propagation directions of the ballistic wave and sea swell. It is illustrated in Fig. 4b, where the mode amplitude is shown as a function of frequency and grazing angle of the ballistic wave, when the sea swell travels at 45° angle to $\mathbf{q}_{in}$. In terms of variables Y_j introduced in Eq. (34), a resonance occurs when either $Y_1 = 0$ or $Y_2 = 0$. The *T*-phase spectrum and resonance frequency for each normal mode also depend on the swell wavelength $\lambda_{sw} = 2\pi/\mu$. Longer λ_{sw} favors excitation of lower-frequency *T*-waves (Figs. 4c and 4d). The same swell wavetrain generates lower-frequency *T*-waves, when it is located around the epicenter (Fig. 4c) than away from it (Fig. 4d). If sea swell with the same wavelength and propagation direction is present in a large area with dimension comparable to the hypocenter depths, the resonantly excited normal mode is received at different frequencies at the observation points that are located at different azimuthal directions from the epicenter. Note also that, according to Eq. (34), any swell wavetrain resonantly scatters the ballistic waves of the compressional and shear-wave origin in different azimuthal directions and at different frequencies.

According to Eqs. (33) and (34), the magnitude squared of the amplitude of *n*th normal mode generated at scattering by sea swell is

$$\left|Q_n^2\right| = \frac{32\pi^3\xi_n}{\xi_n^2 - q_{in2}^2}\left|\frac{\partial P}{\partial z}\right|^2 \left|\Phi\left(q_{in1} - \sqrt{\xi_n^2 - q_{in2}^2}\,\frac{x - x_0}{\left|x - x_0\right|}\right)\right|^2, \tag{35}$$

where

$$\Phi\left(q_1\right) = \frac{iL\sigma_\eta}{2^{3/2}\pi} e^{-iq_1x_0} \left.\frac{\sin Y}{Y}\right|_{Y=(q_1-\mu)L/2}^{Y=(q_1+\mu)L/2} \tag{36}$$

is the one-dimensional wavenumber spectrum of the surface elevation due to swell, Eq. (29), viewed as a function of x. We show below that same result for $\left|Q_n^2\right|$ can be formally obtained from the results that have been derived in Sec. II B for random sea surface roughness, if one uses

$$S_\eta\left(q_1, q_2\right) = \frac{8\pi}{L}\left|\Phi\left(q_1\right)\right|^2 \delta\left(q_2\right) \tag{37}$$

for the swell power spectrum in Eq. (17). Here, $\delta(\cdot)$ denotes the Dirac delta function. It originates from the surface elevation being independent of coordinate y. We assume here that σ_η is independent of coordinates. We will also assume for simplicity that variations of $\mathbf{q}_{in}$ and $\partial P/\partial z$ in the incident wave are negligible within the swell wave train.

In the integrand in the right side of Eq. (17) $q_2 = \xi_n\left(y - y_3\right)\left|\mathbf{r} - \mathbf{r}_3\right|^{-1} - q_{in2}$, and $q_2 = 0$ when $y_3 = y_{1s}$, see Eq. (31). Then, $\left|\mathbf{r} - \mathbf{r}_3\right| = \left|x - x_3\right|\left(1 - \xi_n^{-2} q_{in2}^2\right)^{-1/2}$ and

$$\delta(q_2)=\left|\frac{\partial}{\partial y_3}\left(\xi_n\frac{y-y_3}{|\mathbf{r}-\mathbf{r}_3|}-q_{in2}\right)\right|^{-1}\delta(y_3-y_{1s})=\frac{\xi_n^2|x-x_3|}{\left(\xi_n^2-q_{in2}^2\right)^{3/2}}\delta(y_3-y_{1s}). \qquad (38)$$

Inserting Eqs. (37) and (38) in the integrand in Eq. (17) and integrating first over y_3 and then over x_3 gives Eq. (35). Note that this derivation of Eq. (35), like Eq. (17), apply in the far field with respect to the correlation scale of the sea surface roughness. This is a very significant limitation in the case of swell. No such assumption was made in the derivation of Eq. (33), which is applicable everywhere outside the swell wavetrain itself.

To elucidate the relative significance of wind seas and swell in the abyssal T wave problem, let us compare the acoustic power fluxes J_n in the normal modes generated at sound scattering by two types of ocean surface roughness in the same area $|x–x_0| \leq L/2$ of the ocean surface. For simplicity, we will disregard dependence of $\partial P/\partial z$ on x and variation of $\mathbf{q}_{in}$ and wind wave spectrum with coordinates within the area that contributes the most to the scattering. Then, Eq. (19) gives

$$\langle J_n\rangle=\frac{\pi^2E}{2\omega}L\tilde{S}_\eta, \quad E=\left(\frac{1}{\rho}\frac{\partial f_n}{\partial z}\right)^2_{z=0}\int_{-\infty}^{+\infty}\left|\frac{\partial P}{\partial z}\right|^2 dy \qquad (39)$$

for wind seas. Here, $\tilde{S}_\eta$ is the value of the wind wave spectrum at some point within the integration domain in Eq. (19). [Equation (39) follows immediately from application of the first mean value theorem for integrals to the right side of Eq. (19).] $\tilde{S}_\eta$ in Eq. (39) can be viewed as a weighted average of the spectrum S_η over the horizontal direction of the mode propagation within the interval $|\xi_n - q_{in}| < q < \xi_n + q_{in}$ of wavenumbers q of wind seas. This interval contains all possible $q = |\xi_n\mathbf{e} - \mathbf{q}_{in}|$ in the integrand in Eq. (19). When the peak $q = q_p$ of the wave spectrum lies within the interval $|\xi_n - q_{in}| < q < \xi_n + q_{in}$, $\tilde{S}_\eta \sim q_p^{-2}\sigma_\eta^2/2\pi$ according to Eqs. (27) and (28); $\tilde{S}_\eta$ is small otherwise.

For scattering by swell, acoustic power flux in a normal mode can be calculated by integrating the x component of the acoustic power flux density along the vertical planes $x - x_0 =$ const. $> L/2$ (toward increasing x) and $x - x_0 =$ const. $< -L/2$ (toward decreasing x). Similar to derivation of Eq. (18), from Eqs. (9) and (33) we find

$$J_n = \frac{\xi_n L^2}{16\omega\left(\xi_n^2 - q_{in2}^2\right)}\left(\frac{1}{\rho}\frac{\partial f_n}{\partial z}\right)_{z=0}^2 \int_{-\infty}^{+\infty}\sigma_\eta^2\left(\frac{\sin Y_2}{Y_2} - \frac{\sin Y_1}{Y_1}\right)^2\left|\frac{\partial P}{\partial z}\right|^2 dy \qquad (40)$$

for the power flux toward increasing x. $Y_{1,2}$ in Eq. (40) are given by Eq. (34) with $(x - x_0)/|x - x_0| =1$. The power flux toward decreasing x is given by the same Eq. (40) but now with $(x - x_0)/|x - x_0| = -1$ in Eq. (34) for $Y_{1,2}$.

Resonant excitation of nth acoustic normal mode at scattering by swell occurs when one of the four conditions, $q_{in1} \pm \sqrt{\xi_n^2 - q_{in2}^2} \pm \mu = 0$, is met. Then, one of the $Y_{1,2}$ values in Eq. (40) is zero. Near the resonance frequency [more specifically, as long as $\left|Y_{1,2}\right|$ is either small or $O(1)$], the term in parenthesis in the integrand in the right side of Eq. (40) is $O(1)$, and $J_n \sim EL^2\sigma_\eta^2/8\omega\xi_n$. Note that J_n is proportional to L^2 due to coherent scattering of sound by the swell wavetrain. Away from the resonance frequencies, when all $|Y_j| \gg 1$, J_n decreases by the factor of the order of $\mu^2L^2 \gg 1$. For the contribution of wind seas, Eq. (39) gives $\left\langle J_n\right\rangle \sim \pi EL\sigma_\eta^2/2\omega\xi_n^2$, when the peak of the wind wave spectrum fully contributes to generation of nth normal mode. As expected, $\left\langle J_n\right\rangle$ is proportional to the area occupied by surface roughness and, hence, to L at incoherent scattering of sound by random surface waves.

Aside from the roughly estimated numerical factors, in the vicinity of resonance frequencies the energy of swell contribution to *T*-phase exceeds the maximum contribution of wind waves with the same wave height by the factor $\xi_n L \gg 1$. Thus, *T* waves due to swell can dominate over the wind-wave contribution in narrow frequency bands not only in specific directions but also in the azimuthally integrated power flux, even when the local winds are strong and the peak of the wind wave spectrum $q_p \sim \mu$. However, according to Eq. (40), only a narrow vicinity $\delta f \sim c/L$ of the resonant frequency contributes significantly to the energy of sound scattered by swell, and the broadband acoustic power fluxes due to scattering by wind waves and swell with the same wave height prove to be comparable.

C. Dependence of *T*-phase energy and duration on the hypocenter depth

Calculation of the *T*-wave spectrum with Eqs. (17) and (33) requires knowledge of the distribution of wind speed and sea swell in an area around earthquake epicenter as well as a model of the ballistic waves generated by the earthquake. In this section, we use a basic model of the seabed and simplified, semi-quantitative versions of the theoretical results for mode amplitudes in order to estimate the dimensions of the area of the ocean surface, where *T* waves are generated, and understand the variation of the abyssal *T*-phase duration and energy with the depth of earthquake focus. For these estimates, the seabed is modeled as a homogeneous solid half-space with the density and elastic parameters of the Earth's crust near the earthquake focus, and a compact, directional seismic source is supposed to be located at the focus. For orientation, c_l = 8 km/s, c_t = 4 km/s, and M = 3 can serve as representative values of the compressional and shear wave speeds and the ratio of the densities of earth's crust and sea water, respectively. The hypocenter (focus) of the earthquake is at the point (0, 0, $H + D$) at depth D below the seafloor

(Fig. 1). The source will be characterized by the frequency-dependent amplitudes A_P and A_{SV} and corresponding directional factors $B_P(\theta, \varphi)$ and $B_{SV}(\theta, \varphi)$ of compressional (P) and vertically polarized shear (SV) waves that are radiated by the earthquake. Horizontally polarized shear waves in the crust do not contribute to acoustic field in water.[62] By definition, $|B_P| \le 1$ and $|B_{SV}| \le 1$. When considering the incident waves that are scattered at the ocean surface, we focus on the ballistic waves arriving directly from the source and disregard the weaker arrivals, which reach the ocean surface and are scattered after previously undergoing surface and bottom reflections.

Parameters of the incident acoustic wave, which is scattered by the rough ocean surface, affect the wind wave contribution to T-phase mode amplitudes, Eq. (17), via $\partial P/\partial z$ and $\mathbf{q}_{in}$. The amplitude and the angle of incidence of the incident wave vary along the ocean surface. With wind waves being independent from the focal depth and the other earthquake properties, after averaging over wind speeds and directions, Eq. (17) can be written as follows:

$\left\langle \left| Q_n^2 \right| \right\rangle = 4\pi^2 r^{-1} \left\langle S_\eta \right\rangle \Psi$, where

$$\Psi = \int \left| \partial P(\mathbf{r}_3, 0)/\partial z \right|^2 d\mathbf{r}_3. \quad (41)$$

The average $\left\langle S_\eta \right\rangle$ of the wind wave spectrum is largely insensitive to the angle of incidence of the ballistic waves from the earthquake. For instance, it follows from Eqs. (27) and (28) that $\left\langle S_\eta \right\rangle \sim q_p^{-2}\sigma_\eta^2 / 2\pi$ and is controlled by the representative wind speed alone, when the peak of the wind wave spectrum contributes to T-phase generation. Hence, the effect of the earthquake parameters on T-phase generation is characterized by the surface integral Ψ in Eq. (41).

Averaging Eq. (40) over the swell wavelength and wave trains' location and propagation direction shows that Ψ Eq. (41) also encapsulates the effect of the incident wave on T-phase generation due to sound scattering by sea swell.

For the steep angles, at which ballistic waves from the earthquake propagate in the water column, variations of the sound speed in water with depth are insignificant. Sound speed c and density ρ in water will be assumed constant in the analysis of the ballistic waves. Then, using the results for spherical wave transmission through a plane interface of two homogeneous media,[55] we find

$$\frac{\partial P(\mathbf{r},0)}{\partial z} = -\frac{i\omega}{c} A_P B_P(\theta_l,\varphi) T_l(\theta_l)\left[\frac{\sin\theta_l}{r}\Big/\left(\frac{D}{\cos^3\theta_l}+\frac{cH}{c_l\cos^3\theta}\right)\right]^{1/2} \times\exp\left[i\omega\left(\frac{D}{c_l}\cos\theta_l+\frac{H}{c}\cos\theta\right)-\frac{\alpha_l D}{\cos\theta_l}\right] \quad (42)$$

at the point $\mathbf{r} = r(\cos\varphi, \sin\varphi, 0)$ on the ocean surface. Equation (42) describes the contribution of compressional waves in the seabed and is obtained in the ray approximation. Here θ and θ_l are the incidence angles (i.e., the angle ray makes with the z axis) in the ocean and seabed, respectively; α_l denotes attenuation coefficient of compressional waves, and T_l is the plane-wave transmission coefficient of compressional waves at the seafloor. The incident angles are related by Snell's law and can be found from the equations

$$c^{-1}\sin\theta = c_l^{-1}\sin\theta_l, \quad r = H\tan\theta + D\tan\theta_l. \quad (43)$$

When r increases from 0 to infinity, θ_l increases from 0 to $\pi/2$ according to Eq. (43), while θ increases from 0 to arcsin(c/c_l). The horizontal wave vector $\mathbf{q}_{in}$, which enters Eqs. (16), (17), and (33), is $\mathbf{q}_{in} = \omega c^{-1}\sin\theta\cdot(\cos\varphi, \sin\varphi, 0)$.

Contribution of shear waves in the seabed into $\partial P/\partial z$ at the ocean surface is given by equations similar to Eqs. (42) and (43), except the SV wave source amplitude A_{SV}, directional factor B_{SV}, and attenuation coefficient α_t should be used instead of A_P, B_P, and α_l. Transmission coefficient T_t of SV waves replaces T_l in Eq. (42). In addition, the shear wave speed c_t and incidence angle θ_t should be used instead of c_l and θ_l in Eqs. (42) and (43). Since $c_l > c_t$, it follows from Eq. (43) that at any $r > 0$ the ballistic waves due to compressional waves in the seabed arrive at the sea surface at steeper angles than the ballistic waves due the shear waves radiated by the earthquake.

In the case of fluid-fluid interfaces, the transmission coefficient[62]

$$T_l\left(\theta_l\right) = 2c\cos\theta_l \big/ \left(c\cos\theta_l + Mc_l\cos\theta\right). \tag{44}$$

At a solid-fluid interface, T_l and T_t are given by more cumbersome equations,[62] but, as in Eq. (44), T_l is proportional to $\cos\theta_l$ and vanishes when $\theta_l \to \pi/2$, while T_t is proportional to $\cos\theta_t$ and vanishes when $\theta_t \to \pi/2$, see equations (4.2.37)–(4.2.42) in Ref. 62. These properties of the transmission coefficients ensure that areas far from the epicenter contribute little to T wave generation. Transmission coefficients $T_l(\theta_l)$ and $T_t(\theta_t)$ have $O(1)$ values for all real θ_l and θ_t, respectively; $T_t(0) = 0$ and $T_t(0)$ is nonzero.

Since the ballistic waves originating from compressional and shear waves in the seabed have distinct horizontal wave vectors $\mathbf{q}_{in}$, the integral Ψ in Eq. (41) should be calculated separately for these incident waves. [The $\mathbf{q}_{in}$ values are close at near-normal incidence of ballistic waves, which occurs in the vicinity $r \ll H + D$ of the epicenter. However, since $T_t(0) = 0$, the amplitude is then negligible of the incident wave due to SV waves in the bottom, and interference of the two incident waves has no effect on T wave generation.] For the compressional wave contribution, from Eqs. (41)–(43) we find

$$\Psi_P = \left|\frac{\omega}{c} A_P\right|^2 \int_{-\pi}^{\pi} \frac{d\varphi}{2} \int_0^{\pi/2} \left|B_P\left(\theta_l,\varphi\right) T_l\left(\theta_l\right)\right|^2 \exp\left(-\frac{2\alpha_l D}{\cos\theta_l}\right) \sin 2\theta_l \, d\theta_l. \tag{45}$$

Equation (43) has been used to change the integration variable in Eq. (41) from r_3 to θ_l. The result for the contribution Ψ_{SV} of the shear waves in the seabed differs from Eq. (45) by the obvious change of notations, which has been discussed above for Eq. (42).

Note that Eq. (45) does not contain ocean depth *H*. Hypocenter depth *D* enters Eq. (45) only via the exponential term that describes wave attenuation in the solid bottom. Thus, our estimates show that the energy of abyssal *T* waves is independent of the ocean depth and is insensitive to the hypocenter depth at such frequencies that wave energy dissipation is weak. This finding is not restricted to the basic ocean and earth's crust model we consider and, by changing the integration variables to ray launch angles, can be extended to stratified seabed as long as the ray-theoretical description of the ballistic waves remains applicable.

The independence or lack of sensitivity of the abyssal *T*-wave energy to *H* and *D* appears counter-intuitive at first. Indeed, according to Eq. (42), amplitudes of the incident waves on the ocean surface rapidly decrease with increasing *H* and *D*. However, the decrease in amplitude is compensated by an increase in the ocean surface area that contributes to *T* wave generation. For instance, if *H* and *D* are increased by the same factor $\beta > 1$ and the ray launch angle θ_l (or θ_t) is kept constant, r in Eq. (43) increase the same factor β. Incident wave amplitude in Eq. (42) is decreased by the factor β as long as the wave dissipation is negligible. The decrease of the integrand in the surface integral for Ψ in Eq. (41) by the factor β^2 is exactly compensated by the increase in $d\mathbf{r}_3 = r_3 dr_3 d\varphi$. This is closely related to the fact that, as long as dissipation is negligible, the energy of body waves (as opposed to interface seismo-acoustic waves) reaching the ocean surface remains unchanged, when depth of a compact seismic source varies.

In addition to *T*-phase energy, signal duration is another important characteristic of *T* waves. At distant receivers, *T*-phase duration is controlled by the seismic event (rupture) duration in the earthquake focus, normal mode dispersion in the oceanic waveguide, and linear dimensions of the region, where *T* waves are generated. Generation of *T* waves due to sound scattering occurs with different efficiency at various points on the ocean surface and tends to gradually decrease with distance from the epicenter. Assuming spatially uniform statistics of surface gravity waves, the effective radius r_g of the of the area around the epicenter, where abyssal *T* waves are generated, can be estimated as follows [cf. Eq. (41)]:

$$r_g = \Psi^{-1} \int r \left| \partial P(\mathbf{r},0)/\partial z \right|^2 d\mathbf{r}. \qquad (46)$$

Much like Ψ_P and Ψ_{SV} above, r_g needs to be estimated separately for the incident waves due to *P* and *SV* waves in the seabed. In terms of r_g, the lower bound of the *T*-phase duration can be roughly estimated as the difference $2r_g/c$ of acoustic travel times from the opposite margins of the region, where *T* waves are generated. Similarly, r_g/c provides an estimate of the rise (onset) time of the envelope of the *T*-phase waveform.

For the ballistic wave due to *P* waves in the seabed, from Eqs. (42), (43), and (46) we find

$$r_g = \left| \frac{\omega}{c} A_P \right|^2 \Psi_P^{-1} \int_{-\pi}^{\pi} d\varphi \int_0^{\pi/2} \left| B_P(\theta_l,\varphi) T_l(\theta_l) \right|^2 \left(\frac{H\cos\theta_l}{\sqrt{c_l^2 c^{-2} - \sin^2\theta_l}} + D \right) \exp\left(-\frac{2\alpha_l D}{\cos\theta_l} \right) \sin^2\theta_l \, d\theta_l. \qquad (47)$$

Derivation of Eq. (47) is quite similar to that of Eq. (45). For the ballistic wave due to *SV* waves in the seabed, the result follows from Eq. (47) after the previously discussed change in notation. The integral in the right side of Eq. (47) and Ψ_P depend on the source directionality and environmental parameters. In the case of an omnidirectional source in a homogeneous medium ($c = c_l$, $T_l \equiv 1$) without dissipation, Eqs. (45) and (47) give $r_g = 0.5\pi(H + D)$. We now show that r_g remains of the order of $H + D$ in the general case, with a possible exception for high frequencies.

Note that the integrands in Eqs. (45) and (47) are small, when either $\sin\theta_l \ll 1$ (because of the factors $\sin 2\theta_l$ and $\sin^2\theta_l$, respectively) or $\cos\theta_l \ll 1$ (because of the transmission coefficient). Hence, $\tan\theta_l = O(1)$ in the range of θ_l that contributes most to the integrals. The integrand in Eq. (47) differs from the integrand in Eq. (45) by the factor $r = H\tan\theta + D\tan\theta_l$, which is of the order of $H + D$, when $\tan\theta_l = O(1)$. Thus, $r_g = O(H + D)$ generally, and our estimates indicate longer abyssal T-phase duration for deeper earthquakes. At sufficiently high frequencies, i.e., when waves are strongly dissipated in the seabed over the path of length D, the exponential factor $\exp\left(-2\alpha_l D/\cos\theta_l\right)$ in the integrands of Eqs. (45) and (47) favors small θ_l. It results in smaller r_g values at higher T-wave frequencies than at lower ones.

Our results indicate, in agreement with observations,[63–66] that the T-phase rise (onset) time increases with the hypocenter depth D. Furthermore, r_g and the rise (onset) time increase with the water depth H. This prediction is opposite to that of the seafloor scattering model by de Groot-Hedlin and Orcutt[40] but agrees with the observations analyzed by Williams et al.[2]

IV. DISCUSSION

A. Comparison to other mechanisms of *T*-phase generation

For scattering of ballistic waves by rough ocean surface to be a significant mechanism of T-phase generation, the resulting T waves should have a sufficiently large amplitude. At the very least, surface scattering should excite acoustic normal modes much more efficiently than these are excited in a horizontally stratified ocean with plane, horizontal boundaries and interfaces.

The direct excitation of the T waves, which have phase and group speeds close to the sound speed c in water, by seismic sources in layered media is very weak because of the exponential attenuation of shape functions of the corresponding normal modes in the seabed.[1, 3, 41] For a rough semi-quantitative estimate of the direct excitation, we model the seabed as a homogeneous fluid half-space with the sound speed $c_b > c$. The seismic wave source is modeled as a point monopole acoustic source with $A = A_0\delta(x)\,\delta(y)\,\delta(z - D)$ in Eq. (3). (The conclusions remain essentially unchanged for the more complicated dipole or quadrupole sources.) From Eqs.

(2), (3), and (6), we find the power flux $J_n^{(D)} = \omega \left| A_0^2 \right| f_n^2 \left(H + D \right) / 8$ in the nth mode, generated in a layered medium by a point source at the earthquake focus. Here A_0 is the source amplitude. Acoustic pressure is evanescent in the seabed: $f_n \left(H + D \right) = f_n \left(H \right) \exp\left(-\omega D \sqrt{c_n^{-2} - c_b^{-2}} \right),$ where $f_n(H)$ can be estimated from Eq. (7): $f_n^2 \left(H \right) \lesssim 2\rho(0)/H$. When estimating $J_n^{(D)},$ one has to use shear wave speed, rather than the larger compressional wave speed, for c_b because evanescent shear waves attenuate more slowly below the seafloor and provide stronger coupling of the seismic source to the normal modes we consider [i.e., a larger value of $f_n(H + D)$].

The resulting expression for the power flux in the normal mode directly excited by the seismic source should be compared to the power flux in the same mode excited due to scattering of ballistic waves at the rough ocean surface. To estimate the average power flux $J_n^{(W)}$ due to scattering by wind waves on the ocean surface, we employ Eq. (19) and the estimates of the spatial average of the surface roughness spectrum $\left\langle S_\eta \right\rangle \sim q_p^{-2} \sigma_\eta^2 / 2\pi = \left(0.091 \right)^2 \sigma_\eta^4 / 2\pi$ (Secs. III A and III C) and the radius of the contributing region on the ocean surface $r_g \sim H + D$ (Secs. III C). For the modal power flux due to scattering by the wind waves, we arrive at the estimate

$$J_n^{(W)} \sim \frac{\pi^2 \omega \sigma_\eta^4 \left(H + D \right)^2 \sin^2 \chi_n}{2\left(0.091 \right)^2 \rho\left(0 \right) c^2 \left(0 \right) H} \left| \frac{\partial P}{\partial z} \bigg|_{z=0} \right|^2 . \qquad (48)$$

In terms of the amplitude A_0 of omnidirectional point source, for ballistic waves on the ocean surface at the epicenter we have $\left| \partial P / \partial z \right| \simeq \omega^2 \rho_b T\left(0 \right) \left| A_0 \right| / 4\pi \left(H + D \right),$ where $\rho_b = M\rho(0)$ is the seabed density and T is the transmission coefficient Eq. (44).

Combining the above estimates, we find

$$F_1 = \frac{J_n^{(W)}}{J_n^{(D)}} \sim \frac{\sin^2 \chi_n}{2(0.091)^2} \left(\frac{\omega \sigma_\eta}{c(0)} \right)^4 \left[\frac{Mc(H)}{c(H) + Mc_b} \right]^2 \exp\left(2\omega D \sqrt{c_n^{-2} - c_b^{-2}} \right) \qquad (49)$$

for the ratio of the acoustic power fluxes in *T* waves at surface scattering and direct excitation in layered waveguide. The ratio F_1 characterizes the relative significance of scattering by wind waves compared to the direct excitation. Note that F_1 rapidly increases with sound frequency, roughness amplitude, and the earthquake focus depth. With $\chi_n \cong 0.1$ rad, $c_n \cong 1500$ m/s, and $c_b \cong 4000$ m/s, Eq. (49) predicts that scattering due to wind waves generates *T* waves *hundreds of dBs* stronger, than the direct excitation, at frequencies as low as 1 Hz and rms surface elevations as small as $\sigma_\eta = 0.3$ m even for rather shallow earthquakes with $D = 10$ km (or at 2 Hz with even smaller $D = 5$ km). Thus, excitation due to surface scattering of ballistic body waves dominates over the direct excitation at all *T*-phase frequencies, as expected.

In a full-wave, 2-D SPECFEM simulation, Bottero[8] compared *T*-phase generation at a large-scale bathymetric feature (a six kilometer-long, 12° bottom slope centered on the earthquake epicenter) with contributions due to sound scattering by a compact scatterer on the ocean surface. The scatterer was intended to roughly represent a large commercial vessel. Bottero found that, in his model, the compact surface scatterers ("ships") were as strong a *T*-wave source as the downslope conversion on the large bathymetric feature.[8] While the target strength of the scatterer in Ref. 8 is much larger than that of actual ships of the same dimensions,[67] the full-wave simulation results[8] are extremely valuable as the first rigorous comparison of the efficiency of surface scattering and downslope conversion as *T*-phase sources. By analytic evaluation of *T*-phase generation by the compact scatterer considered in Ref. 8 and by wind waves, the numerical results[8] have been used to demonstrate[67] that sound scattering by wind waves dwarfs the contribution of scattering by ships in 3-D and can generate *T* waves at least as efficiently as the presumably dominant[3] generation mechanism of the downslope conversion on large bathymetric features.

We now provide a direct, semi-quantitative comparison of the energy of the *T* waves that are generated in a 3-D ocean by either a large bathymetric feature (a seamount) or sound scattering due to gravity waves on the ocean surface. Let an isolated seamount or a small island be located at distance R from the epicenter. The seamount rises from the otherwise horizontal seafloor to the ocean surface. Width of the seamount in the azimuthal direction is l. It is small compared to R and large compared to water depth H and acoustic wavelengths in the *T*-wave frequency band. The surface of the seamount makes angle γ with the horizontal plane. The amplitude of the normal component of the oscillatory velocity of the surface of the seamount differs from the velocity amplitude in the ballistic waves at the ocean surface at the epicenter by the factor $w > 0$, which includes the effects of the geometric spreading and wave attenuation in the bottom. For a seamount at range $R \gg D + H$ from the epicenter, the ratio of the ballistic wave amplitudes at the seamount and on the ocean surface at the epicenter $w \sim \exp(-\alpha R)(H + D)/R$, where α stands for the attenuation coefficient of P or S waves in the seabed.

Consider the vertical cross-section of the ocean from its surface to the foot of the seamount, where it meets horizontal seafloor. In this cross-section, the horizontal component of the particle velocity due to seismic waves of frequency ω in the seamount can be estimated as $v_1 = \frac{2w\sin\gamma}{\omega\rho}\left|\frac{\partial P}{\partial z}\right|\exp\left[i\Phi(z) + i\sqrt{\omega^2 c^{-2} - \beta^2}\,(H-z)\cot\gamma\right]\sin\beta z$, where factor $2i\sin\beta z$ accounts for interference of incident and surface reflected acoustic waves with the vertical wavenumber β, Φ describes variation of the phase of seismic waves along the seamount slope, and $\partial P/\partial z$ is evaluated on the ocean surface at the earthquake's epicenter. Using normal mode orthogonality to find modal components of the horizontal velocity, we obtain

$$J_n^{(SM)} = \frac{4w^2 l \sin^2\gamma}{\omega\xi_n\rho(0)} \left|\frac{\partial P}{\partial z}\right|^2 \left|U_n^2\right|, \tag{50}$$

$$U_n = \sqrt{\rho(0)} \int_0^H dz \frac{f_n \sin\beta z}{\rho} \exp\left[i\Phi + i\sqrt{\omega^2 c^{-2} - \beta^2}\,(H - z)\cot\gamma \right] \tag{51}$$

for acoustic power flux in the *n*th mode generated by oscillations of the seamount surface. Here, we disregarded guided acoustic mode penetration into the seabed and used the mode normalization condition Eq. (7).

Using the Cauchy–Schwarz inequality and the normalization condition Eq. (7), the upper bound of the integral U_n Eq. (51) can be estimated as follows: $\left|U_n^2\right| \le \rho(0)\int_0^H dz\rho^{-1}\sin^2\beta z \simeq H/2$. A more accurate estimate of U_n, which accounts for oscillations of the integrand with z, is

$$|U_n| \sim 2^{-1/2}\left(\omega^2 c^{-2}(0) - \xi_n^2\right)^{-1/4} = \left[2\omega c^{-1}(0)\sin\chi_n\right]^{-1/2}, \tag{52}$$

where χ_n has the meaning of grazing angle at the ocean surface. The estimate Eq. (52) refers to modes with significant amplitudes throughout the water column. At higher frequencies, there may be modes with deep turning points, which are very weakly manifested at the ocean surface and the seafloor. These normal modes are not considered here.

From Eqs. (48), (50) and (52), we find

$$F_2 = \frac{J_n^{(W)}}{J_n^{(SM)}} \sim \frac{\pi^2 R^2 \exp(2\alpha R)\sin^3\chi_n}{4(0.091)^2 lH\sin^2\gamma}\left(\frac{\omega\sigma_\eta}{c(0)}\right)^4 \tag{53}$$

for the ratio of the modal power fluxes due to surface scattering and due to the seamount. The ratio increases with the range R, surface roughness, and, in agreement with observations,[32] with T-wave frequency. It is larger for steeper normal modes (larger χ_n) and smaller for bigger (larger l) and steeper (larger γ) seamounts.

Depending on environmental parameters and wave frequency, F_2 can be large (i.e., surface scattering dominates) or small (i.e., contribution of surface scattering is negligible) compared to unity. Let $\chi_n = 0.1$, $\gamma = 0.4$, $H = 4$ km, the angular azimuthal dimension of the seamount as seen from the epicenter $l/R = 0.1$, and the rms surface elevation $\sigma_\eta = 1$ m. (All angles are in radian). To estimate the attenuation coefficient, we use compressional wave speed of 8 km/s and Q-factor of 400.[68, 69] [Attenuation coefficient equals 27.3 Q_P^{-1} dB per wavelength in a wave with the quality factor Q_P.] Then, according to Eq. (53), surface scattering creates T waves as strong as those due to a seamount at the range $R = 400$ km from the epicenter at the frequency of about 5.0 Hz, with the surface scattering been the stronger T-wave source at higher frequencies. For $R = 600$ km, 300 km, 200 km and 100 km, the transition frequency, at which $F = 1$, shifts to about 3.7 Hz, 6.2 Hz, 8.3 Hz, and 13.5 Hz, respectively.

Because of their shorter wavelength and smaller quality factors, attenuation in the seabed plays a bigger role for shear than compressional waves. Therefore, the ratio F_2 Eq. (53) is larger for the shear-wave contributions of the seamount oscillations. Let the shear wave speed and Q-factor be 4 km/s and 200. Then, Eq. (53) gives rather low transition frequencies of 5.6 Hz, 3.3 Hz, and 2.4 Hz for $R = 100$ km, 200 km, and 300 km, respectively.

It should be emphasized that Eq. (53) provides an estimate, rather than an accurate prediction, of the relative significance of the surface scattering and a large topographic feature as T-wave sources. On the other hand, our estimates of the contribution of the surface scattering are conservative in the sense that sea swell is expected to contribute to T-wave generation at least as much as wind waves (Sec. III B), and that typical values of σ_η are larger for most of the world ocean[45] than the 1 m assumed in our estimates.

Thus, scattering by surface gravity waves is expected to provide a significant contribution to *T*-phase energy, which is comparable to the contribution due to a downslope conversion on a seamount. In addition, being generated around the earthquake epicenter, the surface scattering contribution will generally separate from the bathymetric contributions by its arrival time and azimuth.

B. Extensions of the theory

We have assumed in Secs. II and III that the ocean is range-independent when averaged over time-dependent variations due to surface and internal gravity waves. This assumption may be too restrictive for the entire propagation path to distant receivers from the abyssal *T*-wave generation site in the vicinity of the earthquake epicenter. However, the assumption is sufficient to evaluate the acoustic energy of abyssal *T* waves and its modal distribution in the real ocean. Indeed, outside of the relatively small region, where the *T* waves are generated, acoustic energy of the scattered wave is conserved and is the same in the near field as in the far field, as long as acoustic dissipation is negligible. Normal-mode distribution of the *T*-phase energy also remains unchanged in horizontally inhomogeneous ocean as long as the adiabatic approximation[55] is applicable. After the normal mode amplitudes in the *T*-phase spectrum are calculated as described in Secs. II–III, the field can be readily propagated to long ranges with full account of sound absorption using either the adiabatic approximation, the coupled-mode or parabolic-equation propagation models.

We have focused on contributions of gravity waves in the ocean into *T*-phase generation. However, the theory of excitation of normal modes of the oceanic waveguide by scattering of body waves, as expressed by Eqs. (10), (17), and (26), can be applied to other types of surface and volume scatterers. One important application is to *T*-phase generation at scattering by volume inhomogeneities within the seabed and roughness of the seafloor and sediment layer interfaces. This *T*-phase excitation mechanism has been previously considered[41, 42] for coupling within the discrete spectrum of the seismo-acoustic field. Arguably, the continuous spectrum (ballistic body waves) make a stronger contribution to *T* wave excitation by bottom scattering than the directly excited discrete spectrum modes, especially for earthquakes with deeper foci. Application of the theory developed in this paper would allow one to better constrain the effective sources of *T* waves on the seafloor and within the seabed (including their spatial distribution, directionality, and frequency dependence), which were either not related quantitatively to environmental properties[41] or arbitrarily assigned[22, 39, 40] in previous work.

Our finding that the contribution of the ballistic waves scattering by internal gravity waves into *T*-phase generation is negligible compared to the contribution of the ocean surface roughness does not necessarily mean that volume scattering in the water column plays no role in this problem. At long-range propagation, internal waves contribute to coupling of the modes generated by surface scattering to the modes confined in the SOFAR channel. Furthermore, the water column contains many different types of inhomogeneities in a wide range of spatial scales. Scattering of the infrasound generated by air guns from the thermohaline fine structure is successfully utilized in seismic oceanography to measure physical parameters of the water column.[70, 71] The frequency band and propagation directions of incident waves that are exploited in the seismic oceanography experiments[70, 71] are comparable to those of the ballistic infrasound waves in the ocean due to underwater earthquakes. Thus, seismic oceanography observations suggest that contributions of the fine structure inhomogeneities into scattering of ballistic waves from the earthquakes are non-negligible. Further research is needed to evaluate this mechanism of volume scattering and its possible contribution to *T*-phase generation by volume scattering.

Evers et al.[13] reported observations of *T* waves in the ocean and their atmospheric counterpart, guided infrasonic waves in the atmosphere, which were generated by the same underwater earthquake. Quantitative explanation of the atmospheric observations remains elusive. We hypothesize that, akin to the abyssal *T*-phases, guided infrasonic waves in the atmosphere were excited by the scattering of the earthquake-generated body waves on the rough ocean surface and/or turbulence and internal gravity waves in the atmospheric boundary layer. Although quantitative analysis of the observations[13] is beyond the scope of this paper, it should be noted that Eqs. (10), (17), and (26) can be employed to assess the scattering hypothesis. A distinctive feature of the atmospheric observations by Evers et al.[13] is the low-frequency cutoff in the spectrum of the earthquake-generated infrasound. Observations of the low-frequency cutoff are consistent with predictions of Eqs. (10) and (17), as illustrated in Fig. 3 for *T* waves in the ocean, and provide a strong support for application of the surface scattering hypothesis to atmospheric manifestations of underwater earthquakes.

VI. CONCLUSION

The theory, which is developed in this paper from first principles, offers a quantitative explanation of ubiquitous observations of efficient generation of *T* waves in the vicinity of the earthquake epicenter, including the earthquakes under abyssal plains with relatively smooth seafloor. Wind waves and sea swell on the ocean surface have sufficient amplitudes for *T*-phase excitation and are rich in the spatial scales needed for Bragg scattering of ballistic body waves from the earthquake focus into the acoustic normal modes of the oceanic waveguide.

Surface scattering favors the acoustic modes, which span most of the water column, and is consistent with *T*-wave observations by receivers on the seafloor. Observations of low-frequency cutoff in the *T*-wave spectra find their natural explanation in the spectral properties of the sea surface roughness. Weak correlation between *T*-phase amplitude and hypocentral depth follows directly from a ray representation of ballistic waves in horizontally stratified fluid-solid environment. Ocean surface scattering also offers a simple explanation for observations of the increase of the *T*-phase onset time with the water depth and hypocentral depth.

Contributions of scattering by internal gravity waves into *T*-wave generation are found to be negligible compared to the contributions of surface gravity waves, among which the sea swell is expected to be the biggest contributor. Calculation of the wind-wave contribution to the conversion of the ballistic waves into *T* waves at surface scattering gives the lower bound of the abyssal *T*-wave energy.

Our focus on the gravity wave contributions to *T*-phase generation is not meant to imply that other, previously identified mechanisms are weak or unimportant. To understand the *T*-wave excitation, we suggest to consider sound scattering at the ocean surface in addition to the seafloor scattering and the seismic wave interaction with large bathymetric features. Presumably, depending on the local conditions, either the ocean surface scattering or the seafloor scattering may be the dominant mechanism of abyssal *T*-phase generation or the two mechanisms may provide comparable contributions. The theory developed in this paper is expected to help in identifying the surface scattering contributions in the appropriate *T*-phase data.

Rigorous 3-D, full-wave numerical modeling (e.g., using the SPECFEM approach[12, 17–19]) of *T*-phase in an ocean model, which combines a large bathymetric feature with a realistic representation of the rough ocean surface, appears to be the logical next step in investigation of the ocean surface scattering as a *T*-wave generation mechanism and ascertaining its significance. Further research is also needed to evaluate the significance of sound scattering by the thermohaline fine structure and other water-column inhomogeneities as possible additional sources of abyssal *T* waves and to extend the theory to the atmospheric counterpart[13] of the *T*-phase phenomenon.

ACKNOWLEDGMENTS

This work was supported in part by the Office of Naval Research, awards N00014-17WX00773 and N00014-20WX01312. Helpful discussions with A. Bottero, P. Cristini, L. Evers, and R. A. Stephen are gratefully acknowledged. The author thanks the Associate Editor and three anonymous reviewers for their advice on improving the presentation.

References

[1] I. Tolstoy and M. Ewing, "The T-phase of shallow focus earthquakes," Bull. Seismol. Soc. Am. **40**, 25–51 (1950).

[2] C. M. Williams, R. A. Stephen, and D. K. Smith, "Hydroacoustic events located at the intersection of the Atlantis (30°N) and Kane (23°40'N) Transform Faults with the Mid-Atlantic Ridge," Geochem. Geophys. Geosyst., **7**, Q06015 (2006).

[3] E. A. Okal, "The generation of *T* waves by earthquakes," Advances in Geophysics **49**, 1–65 (2008).

[4] J. S. Buehler and P. M. Shearer, "*T* phase observations in global seismogram stacks," Geophys. Res. Lett. **42**, 6607–6613 (2015).

[5] J. A. Hildebrand, "Anthropogenic and natural sources of ambient noise in the ocean," Mar. Ecol. Prog. Ser., **395**, 5–20 (2009).

[6] W. S. D. Wilcock, K. M. Stafford, R. K. Andrew, and R. I. Odom, "Sounds in the ocean at 1–100 Hz," Annu. Rev. Mar. Sci. **6**,117–140 (2014).

[7] I. F. Kadykov, *Acoustics of Underwater Earthquakes* (Nauka, Moscow, 1986) (in Russian).

[8] A. Bottero, *Full-wave numerical simulation of T-waves and of moving acoustic sources*, Ph.D. thesis, Université Aix Marseille (2018).

[9] F. K. Duennebier and R. H. Johnson, *T-phase sources and earthquake epicenters in the Pacific Basin*. Tech. Report, Inst of Geophysics, Hawaii Univ., Honolulu, 1967. 100 pp.

[10] G. D'Spain, L. Berger, W. Kuperman, J. Stevens, and G. Baker, "Normal mode composition of earthquake T phases," Pure Appl. Geophys. **158**, 475–512 (2001).

[11] S. E. Freeman, G. L. D'Spain, S. D. Lynch, R. A. Stephen, K. D. Heaney, J. J. Murray, A. B. Baggeroer, P. F. Worcester, M. A. Dzieciuch, and J. A. Mercer, "Estimating the horizontal and

vertical direction-of-arrival of water-borne seismic signals in the northern Philippine Sea," J. Acoust. Soc. Am. **134**(4), 3282–3298 (2013).

[12] G. Jamet, C. Guennou, L. Guillon, C. Mazoyer, and J. Y. Royer, "T-wave generation and propagation: A comparison between data and spectral element modeling," J. Acoust. Soc. Am. **134**(4), 3376–3385 (2013).

[13] L. Evers, D. Brown, K. Heaney, J. Assink, P. Smets, and M. Snellen, "Evanescent wave coupling in a geophysical system: Airborne acoustic signals from the Mw 8.1 Macquarie Ridge earthquake," Geophys. Res. Lett. **41**, 1644–1650 (2014).

[14] H. Shimamura, and T. Asada, "T waves from deep earthquakes generated exactly at the bottom of deep-sea trenches," Earth Planetary Sci. Lett., **27**(2), 137–142 (1975).

[15] R. Butler, "Observations of polarized seismoacoustic T waves at and beneath the seafloor in the abyssal Pacific ocean," J. Acoust. Soc. Am. **120**, 3599–3606 (2006).

[16] A. Ito, H. Sugioka, D. Suetsugu, H. Shiobara, T. Kanazawa, and Y. Fukao, "Detection of small earthquakes along the Pacific-Antarctic Ridge from T-waves recorded by abyssal ocean-bottom observatories," Mar. Geophys. Res. **33**, 229–238 (2012).

[17] A. Bottero, P. Cristini, and D. Komatitsch, "Numerical simulations of T-wave generation and conversion at shores: Influence of slope angles and of the SOFAR channel," J. Acoust. Soc. Am. **141**, 4045 (2017).

[18] J. Lecoulant, C. Guennou, L. Guillon, and J. Y. Royer, "Three-dimensional modeling of earthquake generated acoustic waves in the ocean in simplified configurations," J. Acoust. Soc. Am. **146**, 2113–2123 (2019).

[19] A. Bottero, P. Cristini, and D. Komatitsch, “On the influence of slopes, source, seabed and water column properties on T waves: Generation at shore,” Pure Appl. Geophys. **177**, 5695–5711 (2020).

[20] C. G. Fox, R. P. Dziak, H. Matsumoto, and A. E. Schreiner, “The potential for monitoring low-level seismicity on the Juan de Fuca Ridge using military hydrophone arrays,” Mar. Technol. Soc. J. **27**, 22–30 (1994).

[21] D. K. Smith, M. Tolstoy, C. G. Fox, D. R. Bohnenstiehl, H. Matsumoto, and M. J. Fowler, “Hydroacoustic monitoring of seismicity at the slow-spreading Mid-Atlantic Ridge,” Geophys. Res. Lett., 29(11), 1518 (2002).

[22] Y. Yang and D. W. Forsyth, “Improving epicentral and magnitude estimation of earthquakes from T phases by considering the excitation function,” Bull. Seism. Soc. Am. **93**(5), 2106–2122 (2003).

[23] R. P. Dziak, S. R. Hammond, and C. G. Fox, “A 20-year hydroacoustic series of seismic and volcanic events in the northeast Pacific Ocean,” Oceanography **24**(3),280–293 (2011).

[24] H. Sugioka, Y. Fukao, and T. Hibiya, “Submarine volcanic activity, ocean-acoustic waves and internal ocean tides,” Geophys. Res. Lett., **32**, L24616 (2005).

[25] W. Wu, Z. Zhan, S. Peng, S. Ni, and J. Callies, “Seismic ocean thermometry,” Science, **369**(6510), 1510–1515 (2020).

[26] C. Wunsch, “Advance in global ocean acoustics,” Science, **369**(6510), 1433–1434 (2020).

[27] D. A. Walker, C. S. McCreery, and Y. Hiyoshi, “T-phase spectra, seismic moments, and tsunamigenesis,” Bull. Seism. Soc. Am. **82**, 1275–1305 (1992).

[28] F. M. Graeber and P.-F. Piserchia, “Zones of *T*-wave excitation in the NE Indian ocean mapped using variations in backazimuth over time obtained from multi-channel correlation of IMS hydrophone triplet data,” Geophys. J. International, **158**, 239–256 (2004).

[29] N. R. Chapman and R. Marrett, “The directionality of acoustic T-phase signals from small magnitude submarine earthquakes,” J. Acoust. Soc. Am. **119**, 3669–3675 (2006).

[30] N. R. Chapman and R. Marrett, “Reply to “Comment on ‘The directionality of acoustic T-phase signals from small magnitude submarine earthquakes’ [J. Acoust. Soc. Am. **119**, 3669–3675 (2006)],” J. Acoust. Soc. Am. **121**, 1297–1298 (2007).

[31] D. R. Bohnenstiehl, “Comment on ‘The directionality of acoustic T-phase signals from small magnitude submarine earthquakes’ [J. Acoust. Soc. Am. **119**, 3669–3675 (2006)],” J. Acoust. Soc. Am. **121**, 1293–1296 (2007).

[32] F. K. Duennebier, *Spectral variation of the T-phase* Tech. Report (Inst of Geophysics, Hawaii Univ., Honolulu, 1967). 21 pp.

[33] R. H. Johnson, J. Northrop, and R. Eppley, “Sources of Pacific T-phases,” J. Geophys. Res., **68**, 4251–4260 (1963).

[34] J. Talandier and E. A. Okal, “On the mechanism of conversion of seismic waves to and from *T* waves in the vicinity of island shores,” Bull. Seismol. Soc. Am., **88**, 621–632 (1998).

[35] O. A. Godin, “Surface-to-volume wave conversion in shallow water with a gently sloping bottom,” Acoust. Phys. **53**(6), 714–720 (2007).

[36] O. A. Godin, “Surface-to-volume wave conversion in shallow water with a corrugated bottom,” Acoust. Phys. **54**(3), 346–352 (2008).

[37] R. H. Johnson, R. A. Norris, and F. K. Duennebier, Abyssally generated T-phases, in *The Crust and Upper Mantle of the Pacific Area*, ed. by L. Knopoff, C. L. Drake, and P. J. Hart, Am. Geophys. Union Geophys. Mono. No. 12, 70–78 (1968).

[38] R. E. Keenan, L. R. L. Merriam, "Arctic abyssal T phases: Coupling seismic energy to the ocean sound channel via under-ice scattering," J. Acoust. Soc. Am. **89**, 1128–1133 (1991).

[39] C. D. de Groot-Hedlin, and J. A. Orcutt, "Synthesis of earthquake-generated T-waves," Geophys. Res. Lett. **26**(9), 1227–1230 (1999).

[40] C. D. de Groot-Hedlin and J. A. Orcutt, "Excitation of T-phases by seafloor scattering," J. Acoust. Soc. Am. **109**, 1944–1954 (2001).

[41] M. Park, R. I. Odom, and D. J. Soukup, "Modal scattering: A key to understanding oceanic T-waves," Geophys. Res. Lett. **28**, 3401‑3404 (2001).

[42] R. I. Odom and D. J. Soukup, "Modal scattering and T-waves: Sediment amplification and source effects," J. Acoust. Soc. Am., **115**(5), 2445 (2004).

[43] W. J. Pierson and L. Moskowitz, "A proposed spectral form for fully developed wind seas based on the similarity theory of A. A. Kitaigorodskii," J. Geophys. Res. **69**, 5181–5190 (1964).

[44] J. H. G. M. Alves, M. L. Banner, and I. R. Young, "Revisiting the Pierson–Moskowitz asymptotic limits for fully developed wind waves," J. Phys. Oceanogr. **33**(7), 1301–1323 (2003).

[45] A. Semedo, K. Sušelj, A. Rutgersson, and A. Sterl, "A global view on the wind sea and swell climate and variability from ERA-40," J. Climate, **24**(5), 1461–1479 (2011).

[46] S. M. Flatté, R. Dashen, W. H. Munk, K. M. Watson, and F. Zachariasen, *Sound Transmission Through a Fluctuating Ocean,* (Cambridge University Press, Cambridge, 1979), pp. 44–61.

[47] K. L. Polzin and Y.V. Lvov, "Toward regional characterizations of the oceanic internal wavefield," Rev. Geophysics, **49**(4), RG4003 (2011).

[48] A. Sukhovich, J.-O. Irisson, J. Perrot, and G. Nolet, "Automatic recognition of *T* and teleseismic *P* waves by statistical analysis of their spectra: An application to continuous records of moored hydrophones," J. Geophys. Res. Solid Earth, **119**, 6469–6485 (2014).

[49] M. Hall, "Surface-duct propagation: An evaluation of models of the effects of surface roughness," J. Acoust. Soc. Am. **67**(3), 803–811 (1980).

[50] N. S. Gorskaya and M. A. Raevskii, "Multiple scattering of low-frequency sound waves by surface roughness," Sov. Phys. - Acoust. **32**(2), 99–102 (1986).

[51] R. I. Odom, "A coupled mode examination of irregular waveguides including the continuum spectrum," Geophys. J. R. Astr. Soc. **86**(2), 425–453 (1986).

[52] R. A. Vadov, "Acoustic propagation in the subsurface sound channel," Acoust. Phys. **52**(1), 6–16 (2006).

[53] F. G. Bass and I. M. Fuks, *Wave Scattering from Statistically Rough Surfaces* (Pergamon, Oxford, 1979), 525 pp. Chaps. 2, 3, 11.

[54] A. G. Voronovich, *Wave Scattering from Rough Surfaces* (Springer, Berlin, 1989), pp. 73–100.

[55] L. M. Brekhovskikh and O. A. Godin, *Acoustics of Layered Media. 2: Point Sources and Bounded Beams.* 2nd, extended edn. (Springer, Berlin, 1999), pp. 16–20, 108–126, 135–144, 150–168, 263–282, 410–414.

[56] O. A. Godin, "Calculation of amplitudes of acoustic normal modes from the reciprocity principle," J. Acoust. Soc. Am. **119**(4), 2096–2100 (2006).

[57] *Handbook of Mathematical Functions with Formulas, Graphs, and Tables*, Appl. Math. Ser., Vol. 55, edited by M. Abramovitz and I. A. Stegun (Dover, New York, 1965). Sec. 9.1.

[58] O. A. Godin, Acoustic mode reciprocity in fluid/solid systems: implications on environmental sensitivity and horizontal refraction. In: *Theoretical and Computational Acoustics,* ed. by Y. C. Teng et al. (World Scientific, Singapore, 1999), pp. 59–75.

[59] O. A. Godin, “On the possibility of using acoustic reverberation for remote sensing of the ocean dynamics,” Acoust. Phys. **58**(1), 129–138 (2012).

[60] O. A. Godin, “Wave equation for sound in a medium with slow currents,” Dokl. Akad. Nauk SSSR, **293**(1), 63–67 (1987).

[61] M. S. Longuet-Higgins, “Statistical properties of wave groups in a random sea state,” Phil. Trans. Royal Soc. London. Ser. A: Math. Phys. Sci. **312**(1521), 219–250 (1984).

[62] L. M. Brekhovskikh and O. A. Godin, *Acoustics of Layered Media. 1: Plane and Quasi-Plane Waves*. 2nd edn. (Springer, Berlin etc., 1998), pp. 11–24, 87–98.

[63] R. A. Norris and R. H. Johnson, “Submarine volcanic eruptions recently located in the Pacific by SOFAR hydrophones,” J. Geophys. Res. **74**(2), 650–664 (1969).

[64] A. E. Schreiner, C. G. Fox, and R. P. Dziak, “Spectra and magnitudes of T-waves from the 1993 earthquake swarm on the Juan de Fuca Ridge,” Geophys. Res. Lett. **22**(2), 139‑142 (1995).

[65] J. Hildebrand, C. G. Fox, and R. P. Dziak, “A multipath model for *T*-wave generation by seafloor earthquakes,” J. Acoust. Soc. Am., **100**(4), 2639 (1996).

[66] P. D. Slack, C. G. Fox, and R. P. Dziak, “*P* wave detection thresholds, *Pn* velocity estimates, and *T* wave location uncertainty from oceanic hydrophones,” J. Geophys. Res., **104**, 13,061–13,073 (1999).

[67] O. A. Godin, “On the possible role of gravity waves in the ocean in T-phase excitation by earthquakes,” J. Acoust. Soc. Am. **146**(4), 3068 (2019).

[68] Z. A. Der and T. W. McElfresh, “Short-period P-wave attenuation along various paths in North America as determined from P-wave spectra of the SALMON nuclear explosion,” Bull. Seism. Soc. Am., **66**(5), 1609–1622 (1976).

[69] J. P. Montagner and B. L. N. Kennett, “How to reconcile body-wave and normal-mode reference Earth models,” Geophys. J. International, **125**(1), 229–248 (1996).

[70] W. T. Wood, W. S. Holbrook, M. K. Sen, and P. L. Stoffa, “Full waveform inversion of reflection seismic data for ocean temperature profiles,” Geophys. Res. Lett. **35**(4), L04608, (2008).

[71] R. W. Hobbs, D. Klaeschen, V. Sallarès, E. Vsemirnova, and C. Papenberg, “Effect of seismic source bandwidth on reflection sections to image water structure,” Geophys. Res. Lett. **36**(24), L00D08 (2009).